Chapter 4

Switchable Frequency Selective Surface for Wireless Applications

In large buildings and offices, frequency re-use methods are required to enhance the spectral efficiency and capacity of wireless communication systems. This observation has led to the concept of electromagnetic architecture of buildings [109, 110]. Passive bandstop FSSs can be used to enhance the electromagnetic architecture of a building, and hence to improve spectral efficiency and system capacity, but switchable FSSs can provide a better reconfigurable solution. If switchable FSSs are placed in strategic locations of a building, they can be reconfigured remotely and rapidly, which is not possible with passive FSSs [109]. This paper describes an electronically-switchable FSS, with a highly stable frequency response, useful in such applications.

This research is published in journals and conference proceedings as shown below:

Journal Papers

1. **Ghaffer I. Kiani**, Kenneth L. Ford, Lars Olsson, Martin Nilsson, Chinthana Panagamuwa, and Karu P. Esselle, "*Switchable Frequency Selective Surface for Reconfigurable Electromagnetic Architecture of Buildings*", IEEE Transactions

on Antennas and Propagation (Accepted for publication, October 2009).

2. **Ghaffer I. Kiani**, Kenneth L. Ford, Karu P. Esselle, Andrew Weily, Chinthana Panagamuwa, and John Batchelor, "*Single-Layer Bandpass Active Frequency Selective Surface*", Microwave and Optical Technology Letters, Volume 50, Issue 8, August 2008, Pages: 2149-2151.

Conference Papers

1. **Ghaffer I. Kiani**, Karu P. Esselle, Andrew Weily, and Kenneth L. Ford, "*Active Frequency Selective Surface using PIN diodes*", IEEE Antennas and Propagation International Symposium, Honolulu, Hawaii, USA, 9-15 June 2007, Page(s): 4525-4528.

2. **Ghaffer I. Kiani**, Kenneth L. Ford, Karu P. Esselle, and Andrew Weily, "*Oblique Incidence Performance of an Active Square Loop Frequency Selective Surface*", 2nd European Conference on Antennas and Propagation (EuCAP), Edinburgh, UK, 11-16 November, 2007.

3. **Ghaffer I. Kiani**, Karu P. Esselle, Andrew Weily, and Kenneth L. Ford, "*Active Frequency Selective Surface design for WLAN*", 10th Australian Symposium on Antennas, Sydney, Australia, 14-15 February, 2007.

4.1 FSS Modelling

Figure 4.1 shows the front view of an unit cell of the active FSS while Fig. 4.2 depicts the rear view with the dc bias line. The size of the unit cell is 17 $\times$ 17 mm and the square loop aperture width is 0.75 mm. The outer and the inner edge dimensions of the square loop aperture are 16 mm and 14.5 mm, respectively. A small hole with a

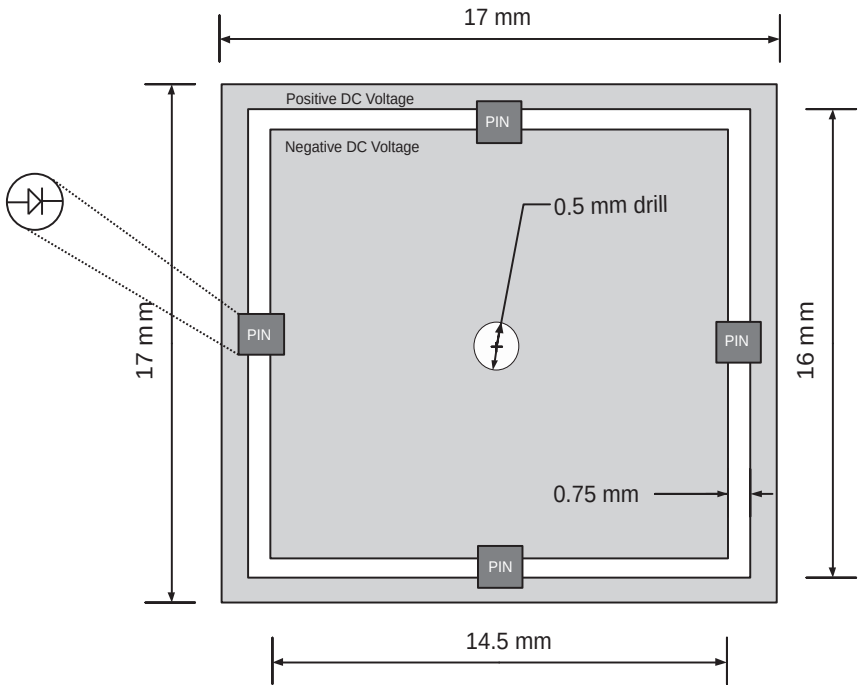

Figure 4.1 The front layout of the unit cell.

0.5 mm diameter is drilled in the centre of the unit cell to provide the negative dc biasing to the PIN diodes. The width of the diagonal dc bias line on the rear surface of the dielectric is 0.5 mm. The periodicity of the elements is 17 mm and there is a 1 mm distance between the outer edges of two adjacent square loops. The dielectric constant of FR4 is chosen as 4 in the simulation. The dimension of the unit cell and square loop is selected in such a way that without the PIN diodes it resonates at a frequency higher than 2.45 GHz. This is due to the fact that, after the PIN diodes are incorporated in the model, the frequency response shifts downwards due to the addition of an appreciable capacitance. CST Microwave Studio (Frequency-Domain Solver) is used to simulate the FSS unit cell.

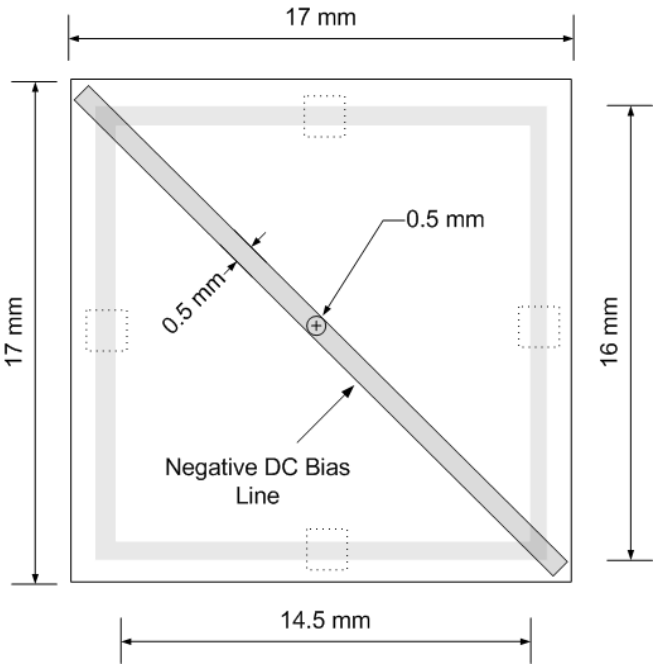

Figure 4.2 The rear layout of the unit cell.

4.2 PIN Diode Modelling

PIN diodes can be modelled as a series RL circuit (for the ON state) and a combination of series-parallel RLC circuit (for the OFF state). Fig 4.3 shows the equivalent circuit models of the PIN diodes in both ON and OFF states [100]. Lumped elements within CST Microwave Studio are used in modelling the PIN diode. Research into several diodes was carried out, and the diode with the most suitable specifications (BAP51-03) was chosen for the project [111]. The criteria for suitable specification were the size, the cost and the least forward resistance of the PIN diode. The Philips BAP51-03 diode has a typical forward resistance of about 5 Ω and has a reasonably low price. The typical values used for forward bias are $R_s = 5\ \Omega$ and $L_s = 0.4$ nH, while for reverse bias a parallel combination of reverse resistance and capacitance is added in series with the resistance and inductance [100]. The value of the capacitance (C_T) is

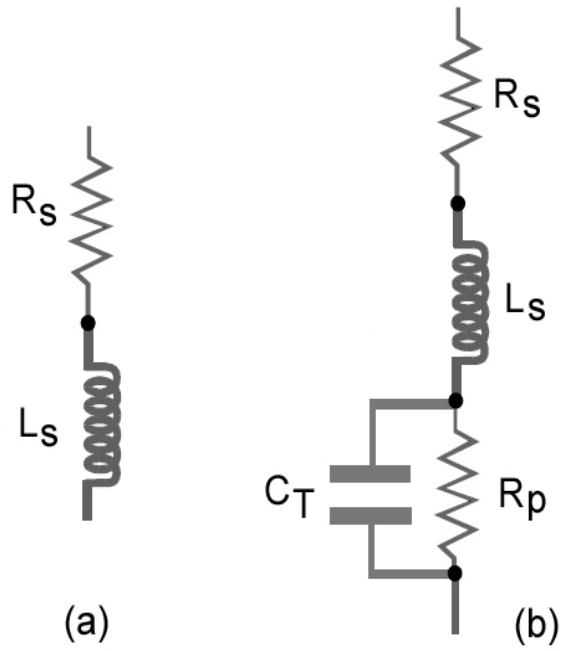

Figure 4.3 (a) Forward-bias and (b) reverse-bias equivalent circuits of the PIN diode used in FSS modelling.

0.2 pF while the reverse resistance (R_p) is 10 KΩ.

4.3 Theoretical Results

In this section theoretical results for the switchable FSS are presented. It can be easily observed that the design has a stable frequency response for both TE and TM polarisations at oblique incidence.

4.3.1 Diodes OFF

Perpendicular (TE) Polarisation

For perpendicular polarisation, the transmission and reflection characteristics of the FSS at 0, 30, 45 and 60 degree incidence angles are shown in Fig. 4.4, when the

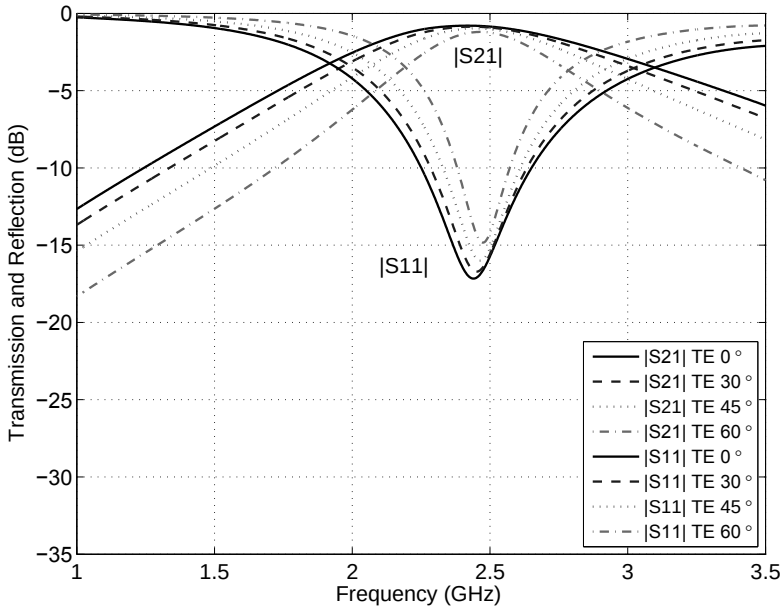

Figure 4.4 Theoretical transmission and reflection characteristics of switchable FSS for perpendicular (TE) polarisation when the diodes are in the OFF state.

PIN diodes are in the OFF state. A stable frequency response can be noticed, as the resonance frequencies for 0, 30, 45 and 60 degree incidence angles are 2.44 GHz, 2.45 GHz, 2.46 GHz and 2.47 GHz, respectively. The reflection coefficients at 0, 30, 45 and 60 degree incidence angles at the resonance frequencies are -17.2 dB, -16.8 dB, -16.1 dB and -14.9 dB, respectively. There is an insignificant reduction in the transmission as the angle of incidence varies from 0 to 60 degrees. The insertion loss in the FSS is mainly due to the presence of the bias lines and PIN diodes. The insertion loss increases slightly as the angle of incidence increases. The insertion loss at 0, 30, 45 and 60 degrees is 0.8 dB, 0.9 dB, 1.0 dB and 1.2 dB, respectively. The -10 dB reflection bandwidth is 402 MHz, 353 MHz, 283 MHz and 192 MHz, respectively. It can be noticed that there is an appreciable reduction in bandwidth as the incidence angle increases from 0 to 60 degrees.

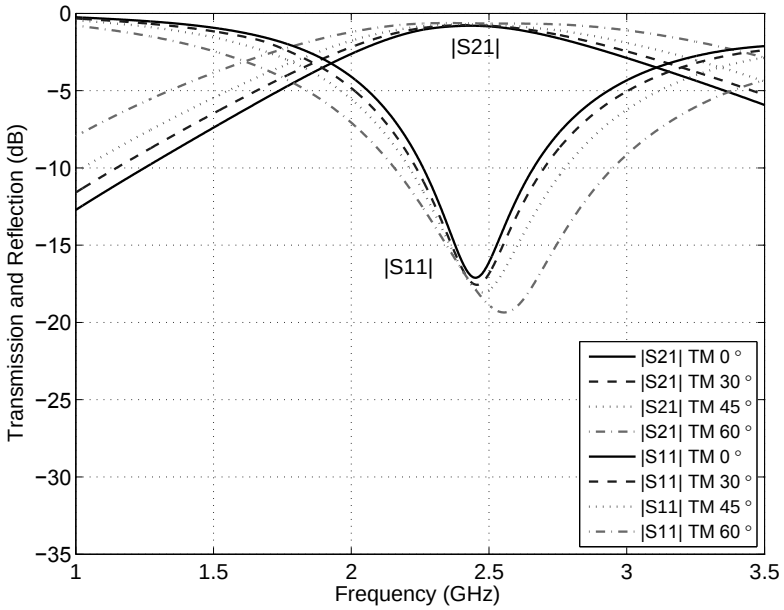

Figure 4.5 Theoretical transmission and reflection characteristics of switchable FSS for parallel (TM) polarisation when the diodes are in the OFF state.

Parallel (TM) Polarisation

For parallel polarisation, the transmission and reflection characteristics of the FSS at 0, 30, 45 and 60 degree incident angles are shown in Fig. 4.5, when the PIN diodes are in the OFF state. A stable frequency response can be noticed in this case as well. The resonance frequencies for 0, 30, 45 and 60 degree incident angles are 2.44 GHz, 2.45 GHz, 2.47 GHz and 2.56 GHz, respectively. The reflection coefficients at 0, 30, 45 and 60 degree incidence angles at the resonance frequencies are -17.1 dB, -17.6 dB, -18.1 dB and -19.5 dB, respectively. The insertion loss in this case is almost constant for all incidence angles considered. The insertion loss at 0, 30, 45 and 60 degrees is 0.7 dB, 0.7 dB, 0.7 dB and 0.6 dB respectively. The -10 dB reflection bandwidth is 402 MHz, 463 MHz, 563 MHz and 797 MHz respectively. In contrast to the perpendicular polarisation (TE) case, there is an appreciable increase in bandwidth as the incidence

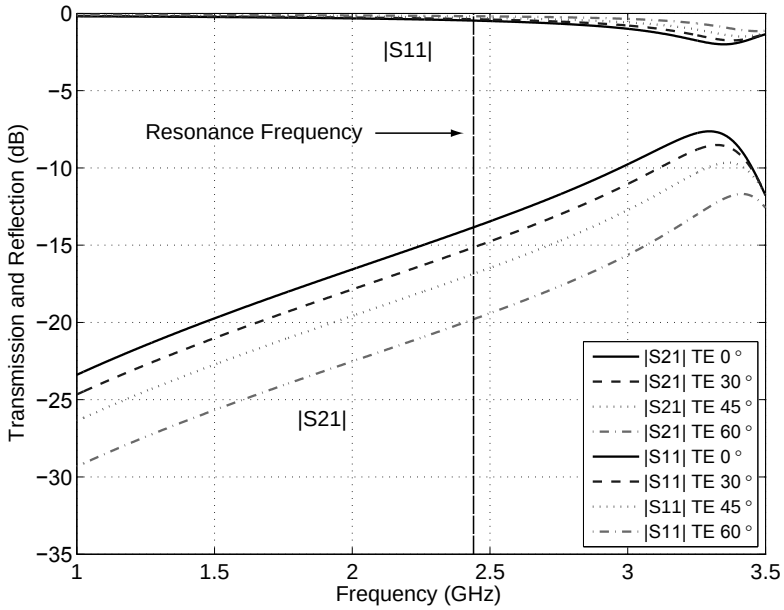

Figure 4.6 Theoretical transmission and reflection characteristics of switchable FSS for perpendicular (TE) polarisation when the diodes are in the ON state.

angle increases from 0 to 60 degrees.

4.3.2 Diodes ON

Perpendicular (TE) Polarisation

For perpendicular polarisation, the transmission and reflection characteristics of the FSS at 0, 30, 45 and 60 degree incidence angles are shown in Fig. 4.6, when the PIN diodes are in the ON state. At 2.45 GHz, the reflection coefficients at 0, 30, 45 and 60 degree angles of incidence are -0.5 dB, -0.4 dB, -0.3 dB and -0.2 dB, respectively. The transmission coefficients are -13.8 dB, -15.1 dB, -16.8 dB and -19.8 dB, respectively, for the angles of incidence considered in this research. The isolation between transmission and reflection states improves as the angle of incidence increases.

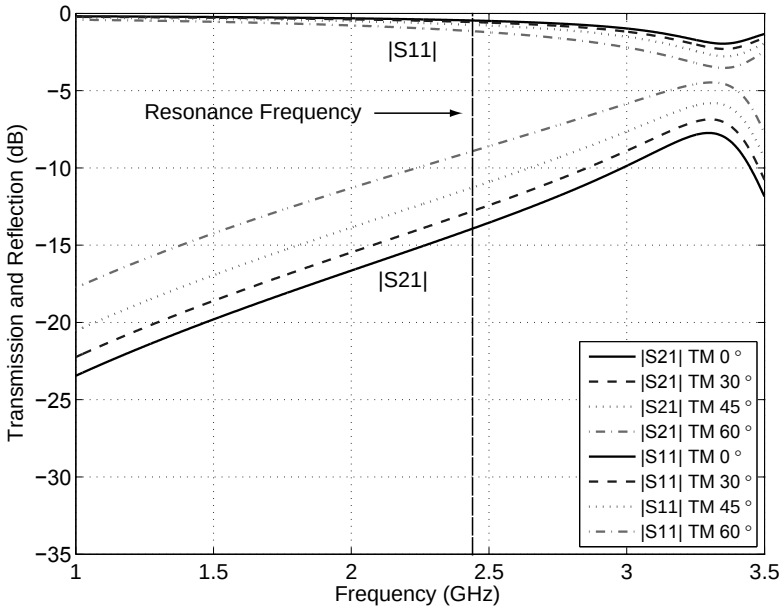

Figure 4.7 Theoretical transmission and reflection characteristics of switchable FSS for parallel polarisation (TM) when the diodes are in the ON state.

Parallel (TM) Polarisation

For parallel polarisation, the transmission and reflection characteristics of the square loop active FSS at 0, 30, 45 and 60 degree incidence angles are shown in Fig.4.7, when the PIN diodes are in the ON state. At 2.45 GHz, the reflection coefficients at 0, 30, 45 and 60 degree incidence angles are -0.5 dB, -0.4 dB, -0.3 dB and -0.2 dB, respectively. The transmission coefficients are -13.9 dB, -12.7 dB, -11.2 dB and -8.9 dB, respectively, for the angles of incidence considered. In contrast to the perpendicular polarisation (TE) case, the isolation between transmission and reflection states in this case decreases as the angle of incidence increases.

Based on this data, it can be seen that, for the TE case, an additional transmission loss of 13 dB, 14.2 dB, 15.7 dB and 18.4 dB can be achieved for 0, 30, 45 and 60 degree angles of incidence, by switching from the ON to the OFF state. The average additional transmission loss is 15.4 dB. On the other hand, the additional transmission

loss for the TM case is 13 dB, 12.1 dB, 10.4 dB and 7.7 dB for the angles of incidence considered. The average additional loss for the TM case is 10.8 dB. The performance is slightly better in the TE case.

It is evident from Fig. 4.5 that the transmission loss for TM polarised waves is independent of the incidence angle at the resonance frequency of 2.45 GHz but, at other frequencies, it decreases with increase in the incidence angle. The reverse is true for the TE case. This happens when the angle of incidence approaches the Brewster angle [108]. When waves move between two plain dielectric media (which do not have a printed metal pattern) of differing refractive index, generally some of the incident power is reflected at the boundary. At one particular angle of incidence, however, waves with parallel polarisation (TM) have a reflection coefficient of zero. This angle of incidence is the Brewster's angle, θ_B and is given as:

$\theta_B = \arctan\ (\eta_2\ /\ \eta_1)$

where η_1 and η_2 are the refractive indices of the two media expressed as:

$\eta = \sqrt{\epsilon_r}\sqrt{\mu_r}$

where ϵ_r is the relative permittivity and μ_r is the relative permeability. Therefore, for this design

$\theta_B = \arctan\ (\eta_2\ /\ \eta_1) = \arctan\ (2/1) = 64^\circ$

This effect contributes to transmission even when the diodes are ON, as seen in Fig. 4.7. It can be noticed that, at a 60 degree angle of incidence, the additional transmission loss for the TM case (between ON and OFF) is 7.7 dB and the transmission coefficient at 2.45 GHz is -8.9 dB. In our bandpass FSS, where the dielectric is covered by an aperture type FSS, there will always be reflection even at the Brewster angle. On the other hand, the additional transmission loss for the TE case is at a maximum at 60 degrees, i.e. 18.4 dB, while the value of the transmission coefficient is -19.8 dB. Therefore, to achieve a better transmission loss for the TM polarised

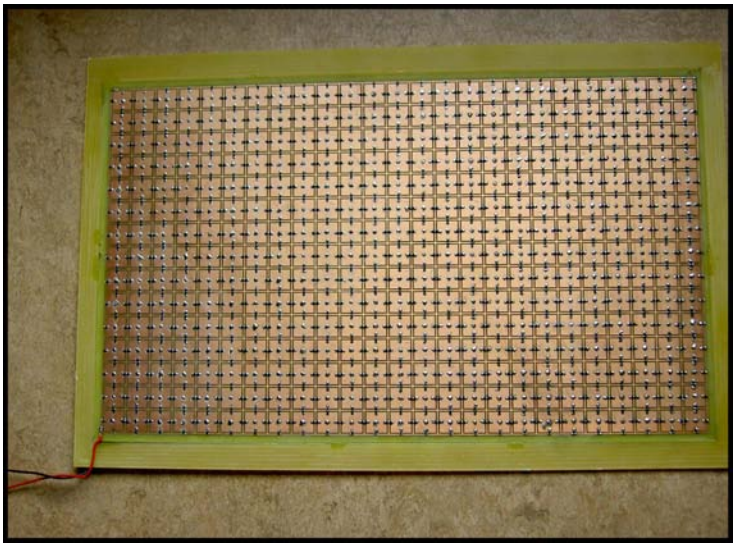

Figure 4.8 The front view of the switchable FSS prototype.

waves at higher angles of incidence, a dielectric material with a high refractive index (and hence a large Brewster angle) must be used. The insertion loss can further be reduced by using a better-quality PIN diode.

4.4 FSS Fabrication

4.4.1 FSS Prototype

An FSS with 25×15 elements has been fabricated using a standard milling process. The overall size of the FSS prototype is 45 cm× 30 cm. The FR4 substrate is 1.6 mm thick, having a relative permittivity of 4. Figs 4.8 and 4.9 show the front and close-up views of the switchable FSS prototype, while Figs 4.10 and 4.11 show the rear and close-up views, respectively. There are four PIN diodes in each unit cell. Positive dc biasing is applied from the front side of the FSS. The diagonal negative dc bias lines on the reverse side are joined together on the border of the FSS prototype.

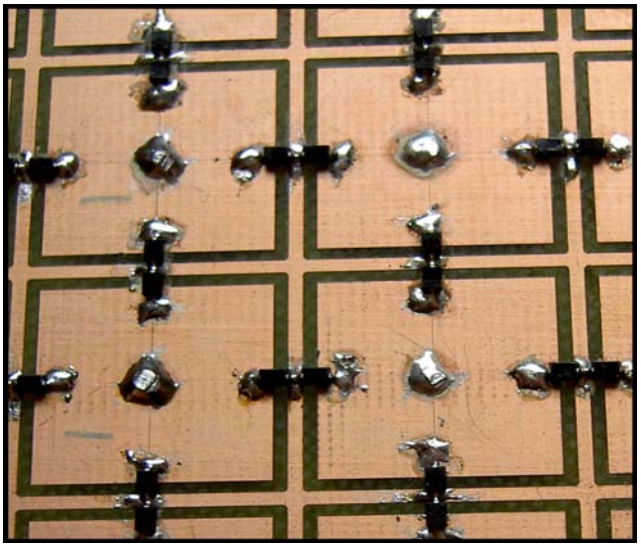

Figure 4.9 The front close-up view of the switchable FSS prototype.

4.4.2 PIN Diode Biasing

A total of 1500 Philips (BAP51-03) [111] diodes were used in the fabrication of the FSS prototype. To switch these PIN diodes from OFF to the ON state, a forward voltage of 2 V was applied to the FSS prototype in both transmission and reflection measurements. A current of approximately 1 A was drawn by the FSS prototype when the diodes were forward biased. No voltage was applied to the diodes in the OFF state.

4.5 Measurement Setup

4.5.1 Transmission

Figure 4.12 shows the measurement setup for switchable FSS prototype. HyperLog 7060 log-periodic antennas from Aariona company were used for measurements [112]. These antennas operate between 700 MHz and 6 GHz and were well suited for the

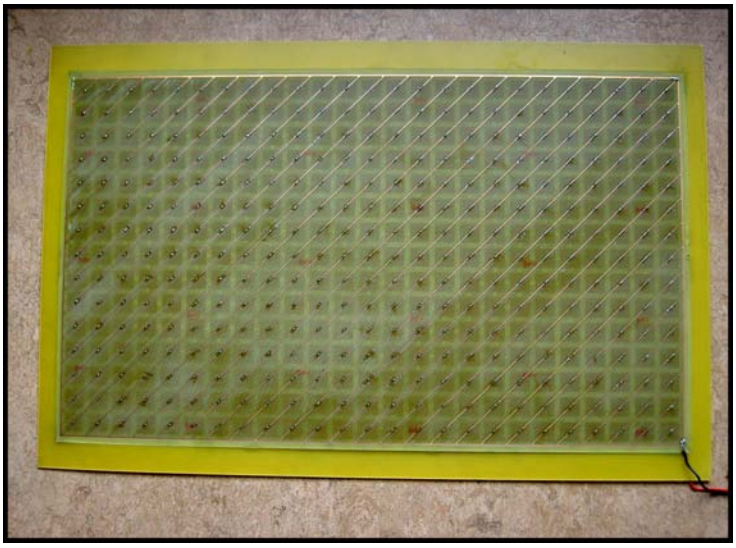

Figure 4.10 The rear view of the switchable FSS prototype.

experimentation. The antennas were connected to the network analyser (Rohde & Schwarz ZVC, 20 kHz to 8 GHz). The transmission was normalised to an open window in a metallic frame and then the FSS prototype was placed in the window to measure the transmission through it. It was observed that there was no major difference in the transmission results whether the measurements were made inside or outside an anechoic chamber. Therefore, for ease of handling, the measurements were performed outside the chamber and the results are presented in Section 4.6. To measure the oblique incidence performance of the FSS prototype, the metallic frame fixed in the wooden stand was rotated anticlockwise by up to 45° from a reference position marked on the floor while the antennas were kept stationary. To measure both TE and TM polarisations, the antennas were rotated around their axes by 90°.

4.5.2 Reflection

Reflectivity measurements were carried out using a standard NRL (Naval Research Laboratory) arch, which is housed within an anechoic chamber. The measurement

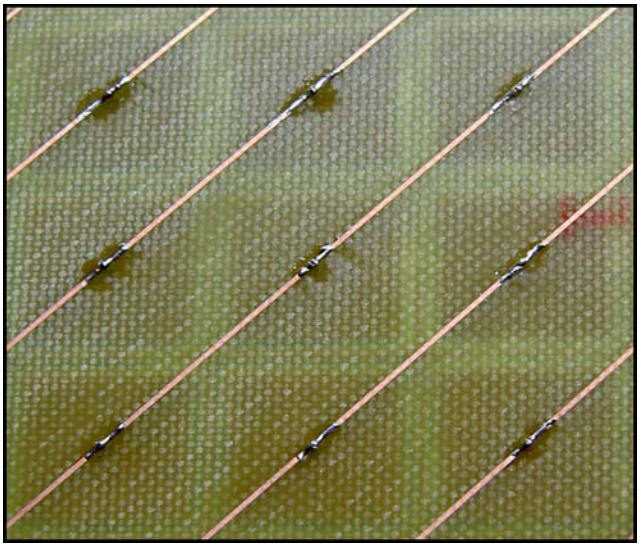

Figure 4.11 The rear close-up view of the switchable FSS prototype.

system is illustrated in Fig. 4.13 and consists of two wide-band horns, covering 2-18 GHz, connected to an HP8510C vector network analyser (VNA). The switchable FSS sample under test was supported on a low-density expanded polystyrene table, which was surrounded by 12 inch pyramidal absorbers. The system was calibrated using a response/isolation technique. The isolation measurement was carried out by first removing the polystyrene table and sample so that the horns were illuminating the chamber absorber directly. For the response measurement the table was replaced and a metal plate was positioned so that its centre was on the axis of rotation of the arch arms which carry the wide-band horns. This resulted in a calibration which gave a noise floor of better than -55 dB across the entire frequency range and this was deemed sufficient to assess the performance of the FSS. To improve the measurements further, the time-domain gating feature within the VNA was used to reduce any effects from erroneous scattering. In order to carry out oblique incidence measurements the supporting arms of the arch were rotated to the appropriate angle using accurate predetermined fixings, and the horns were rotated through 90° each, depending on

Figure 4.12 The transmission measurement setup showing the switchable FSS fixed in a metallic frame between two log-periodic antennas.

the polarisation needed. The previously described calibration was repeated for each angle and polarisation. The inside view of the anechoic chamber for the reflection measurement setup is shown in Fig. 4.14.

4.6 Measured Results

4.6.1 PIN Diodes OFF

Perpendicular (TE) Polarisation

Figure 4.15 shows the measured transmission and reflection characteristics at 0°, 30° and 45° incidence angles for perpendicular polarisation (TE incidence) when the PIN diodes are in the OFF state. The resonance occurred at 3.2 GHz for 0°, with a -17.5 dB reflection. The insertion loss at this frequency for 0° is 2.6 dB. At 30° and 45° incidence angles, the resonance frequency shifts slightly downward to 3.1 GHz and 3.05 GHz, respectively, both with a reflection coefficient of -14 dB. The insertion

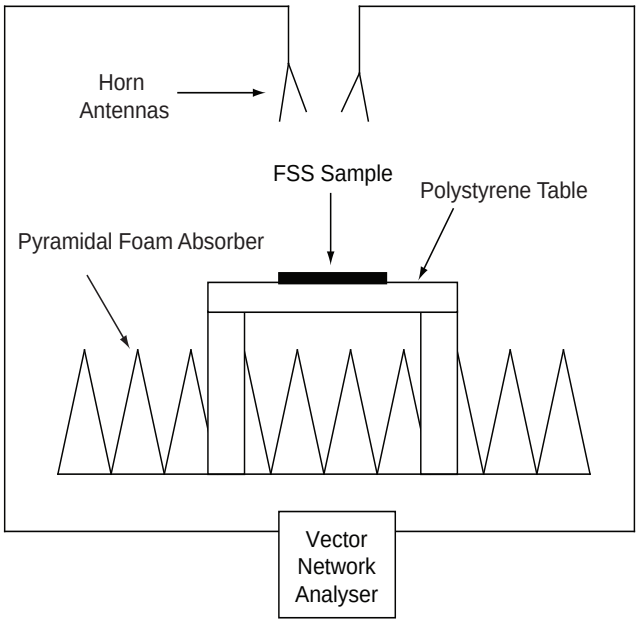

Figure 4.13 Block diagram showing the reflection measurement setup.

losses for these incidence angles are 2.6 dB and 2.6 dB, respectively. Comparing the theoretical results with Section 4.5, the measured resonance frequency is shifted upwards by about 0.5 GHz. The average transmission loss in theory is 0.7 dB as opposed to 2.6 dB in measured results. There are three main causes for the higher values of the measured transmission loss: dielectric losses, diode losses and reflection losses due to the physical presence of the diodes and the soldering material on the FSS surface. The shift in resonance frequency from 2.45 GHz (theoretical) to 3.2 GHz (measured) may be due to: (a) a lower value of dielectric constant of the substrate used for the fabrication of the active FSS; (b) inaccuracies in the parameter values in the diode model; (c) extra inductance added by the dc inter-connecting lines on the border of the finite FSS (rear side); and (d) the soldering material used in the FSS fabrication. The small change in resonance frequency with incidence angle, noticed in measurements, is due to fabrication tolerances.

Figure 4.14 Inside view of the anechoic chamber for the reflection measurement setup.

Parallel (TM) Polarisation

Figure 4.16 shows the measured transmission and reflection characteristics at normal and oblique incidence angles for parallel polarisation (TM incidence). The resonance and insertion loss at normal incidence are the same as in the TE case, as expected from the symmetry of the unit cell. The change in the resonance frequency is also the same as in the TE case while the reflection coefficients at 30° and 45° are -21 dB and -28 dB, respectively. The transmission losses for these angles of incidence are 2.4 dB and 2.3 dB (due to the Brewster effect), respectively.

4.6.2 PIN Diodes ON

Perpendicular (TE) Polarisation

Figure 4.17 depicts the measured transmission and reflection coefficients for perpendicular (TE incidence) polarisation when the diodes are in the ON state. For 0°, 30° and 45° incidence angles, the reflection coefficient is close to -1 dB while the trans-

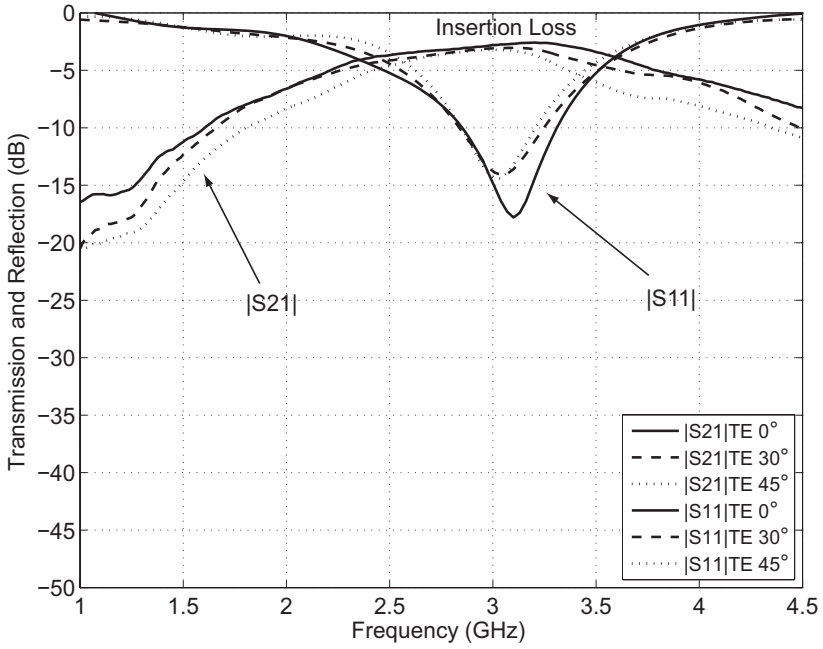

Figure 4.15 Measured transmission and reflection characteristics of switchable FSS for perpendicular polarisation (TE) when the diodes are in the OFF state.

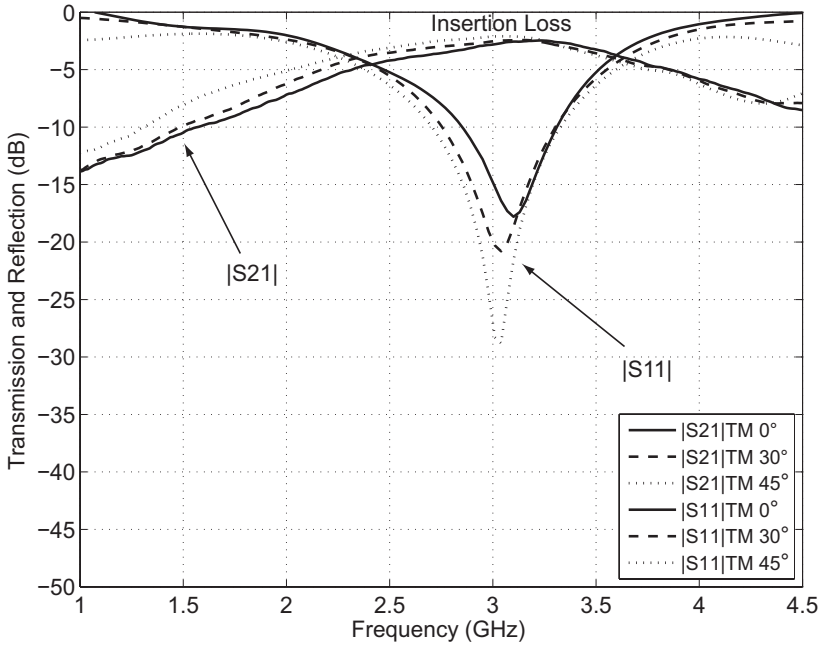

Figure 4.16 Measured transmission and reflection characteristics of switchable FSS for parallel polarisation (TM) when the diodes are in the OFF state.

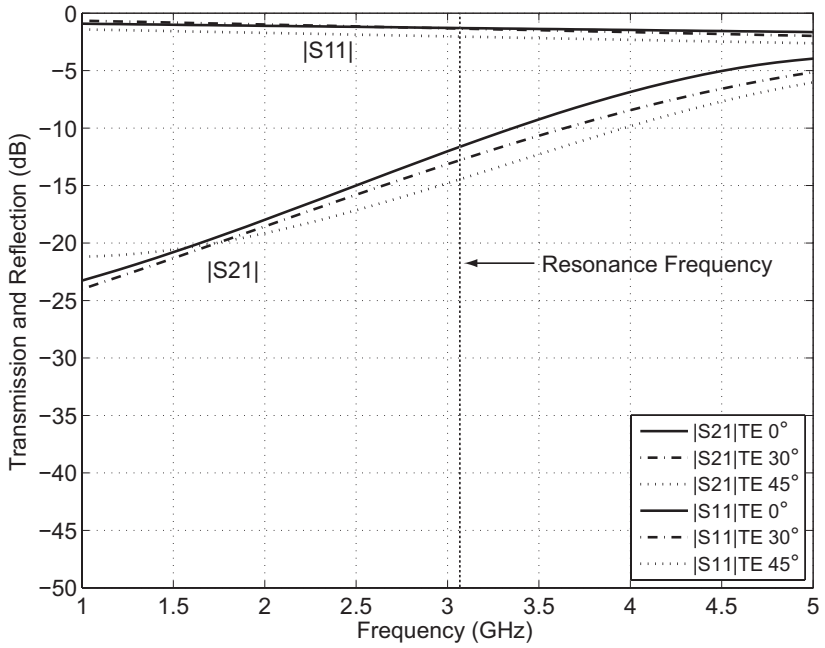

Figure 4.17 Measured transmission and reflection characteristics of switchable FSS for parallel (TM) polarisation when the diodes are in the ON state.

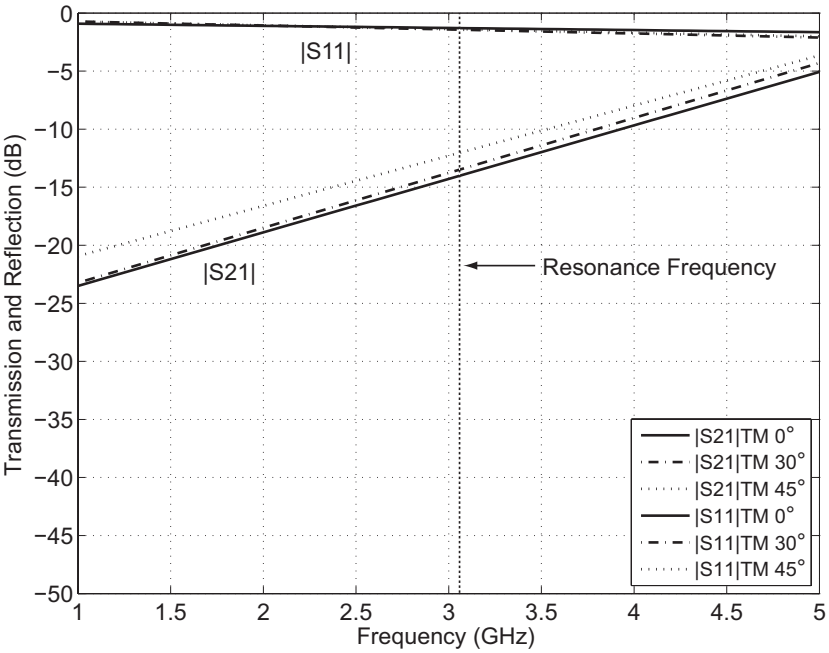

Figure 4.18 Measured transmission and reflection characteristics of switchable FSS for parallel polarisation (TM) when the diodes are in the ON state.

mission loss is 11.5 dB, 13 dB and 14.6 dB, respectively. Therefore, at 0°, 30° and 45° incidence angles, the transmission loss can be switched by 8.9 dB, 10.4 dB and 12.0 dB, respectively, by switching the PIN diodes from OFF to the ON state.

Parallel (TM) Polarisation

Figure 4.18 depicts the measured transmission and reflection coefficients for perpendicular (TM incidence) polarisation. For 0°, 30° and 45° incidence angles, the reflection coefficient is close to -1 dB while the transmission loss is 14 dB, 13.5dB and 12.2 dB, respectively. Therefore, at 0°, 30° and 45° incidence angles, the transmission loss can be changed by 11.4 dB, 11.1 dB and 9.9 dB, respectively, by switching the PIN diodes from OFF to the ON state.

4.7 Circular Loop Aperture FSS

A switchable FSS with a different configuration is described in this section. This FSS is based on a circular loop aperture geometry, with each unit cell having four PIN diodes across the aperture at 90-degree intervals. It shows good angle of incidence stability for perpendicular polarisation (TE) at 2.45 GHz, which is the centre of the IEEE 802.11 b/g WLAN band. The PIN diodes have been placed orthogonal to each other to provide oblique incidence stability at the resonance frequency. Cross-shaped narrow metallic lines are made on the back side of the substrate to provide negative dc biasing, while the positive dc biasing is provided from the front side of the printed structure. It is shown that, experimentally, almost 12 dB of additional transmission loss can be achieved at the resonance frequency by switching the PIN diodes to ON from the OFF state.

4.8 Active FSS Modelling

The front and the rear views of the active circular FSS unit cell are shown in Figs 4.19 and 4.20. The single-layer active FSS is designed on a low-cost FR4 substrate. A circular aperture is used as the FSS element to obtain a good angle-of-incidence stability. The dimensions of the circular aperture are selected in such a way that the unloaded aperture resonates at a higher frequency (2.6 GHz) than the nominal operating frequency (2.45 GHz). The reason for this is that the incorporation of the PIN diodes in the periodic structure adds extra reactance to the bandpass FSS and hence lowers the resonance frequency. Four diodes are placed orthogonally to each other on an unit cell of the FSS to obtain a stable frequency response at oblique TE incidence. The outer and the inner edge diameters of the circular loop aperture are 26.6 mm and 25.6 mm, respectively. This makes the width of aperture 0.5 mm. The outer diameter is approximately half the guided wavelength at 2.6 GHz. The distance between the centres of two adjacent FSS elements is 30 mm. The single-layer active FSS was fabricated on a 420 $\times$ 270 mm^2 FR4 sheet (15 $\times$ 9 elements) with dielectric constant of 4 and 1.6 mm thickness.

The inter-element spacing is kept small to enhance the angle-of-incidence stability [1]. Negative dc biasing is provided from the reverse side of the dielectric substrate by means of symmetrical cross-shaped bias lines. Their width is 0.5 mm. They are aligned with the orthogonal position of the PIN diodes on the front side of the unit cell as shown in Fig. 4.20. The metallic circular plate on the front side of the unit cell is connected to the centre of cross-shaped negative bias lines with the help of a through pin having a diameter of 0.5 mm. The pin is soldered on both sides to provide an electrical connection. The positive dc biasing is provided from the outer end of the circular-loop aperture on the front side of the FSS.

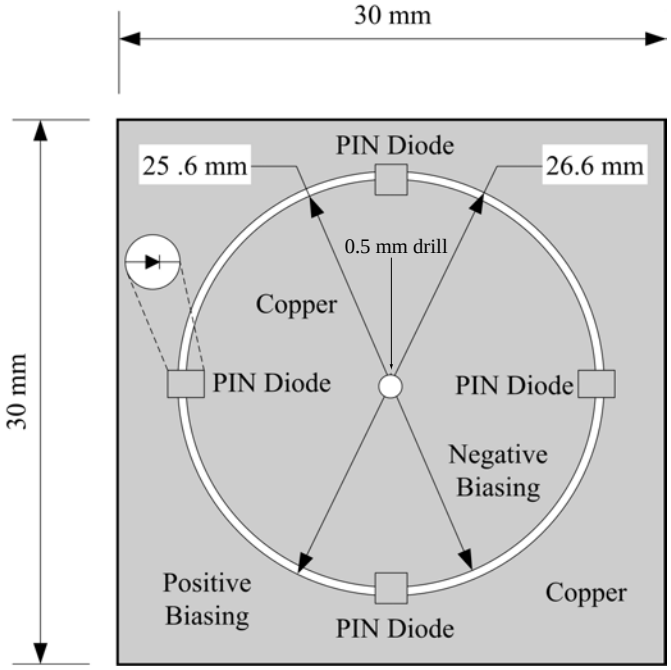

Figure 4.19 Front view of the active circular loop FSS unit cell.

PIN diode modelling and biasing in this case is the same as described in Sections 4.2 and 4.4. The transmission and reflection measurement setup is also the same as described earlier. However, for the transmission measurement, horn antennas were used instead of log-periodic antennas. The fabrication process was also the same as in the case of the square-aperture FSS.

4.9 Theoretical and Measured Results

The FSS unit cell was modelled in CST Microwave Studio using periodic boundary conditions. Fig. 4.21 depicts the results of the simulation, showing the transmission and reflection characteristics of the single-layer active FSS at 0°, 30°, and 45° incidence angles for the TE incidence when the PIN diodes are in the OFF state. The resonance occurs at 2.45, 2.46, and 2.47 GHz for 0°, 30°, and 45° incidences, respectively. As

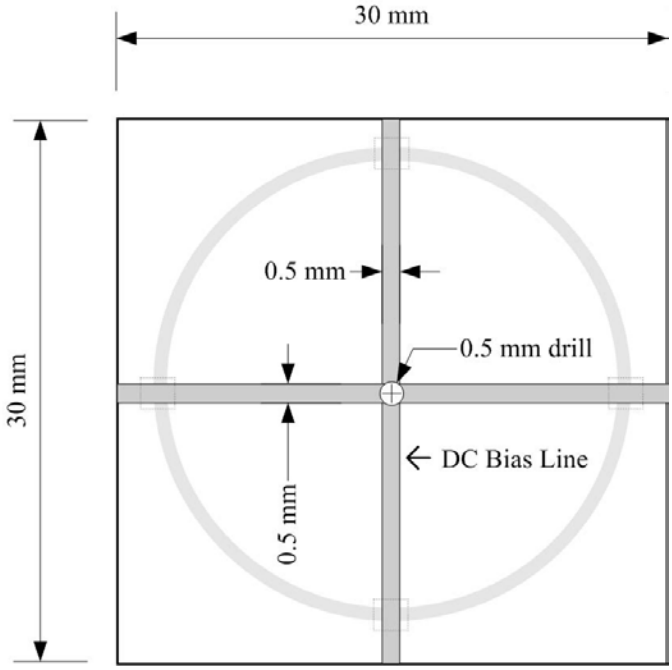

Figure 4.20 Rear view of the active circular FSS unit cell.

far as transmission is concerned, a small insertion loss of 0.5 dB can be noticed for all the incidence angles considered. Fig. 4.22 shows the transmission and reflection characteristics of the FSS in the ON state. The circular apertures are effectively shorted together by the conducting diodes, resulting in an effective conducting sheet. There is no noticeable change in the reflection properties as the angle of incidence is increased from 0° to 45°, while the transmission coefficients change slightly (-17.8 dB to -21.2 dB at 2.45 GHz). Theoretically, an average transmission loss of 19 dB can be achieved at the resonance frequency.

Figure 4.23 shows the measured transmission and reflection characteristics at 0°, 30°, and 45° incidence angles for TE incidence when the PIN diodes are in the OFF state. The resonance occurs at 2.63, 2.64, and 2.65 GHz, respectively, for 0°, 30°, and 45° incidence, while the transmission losses at these angles are 2.7, 2.8, and 3.4 dB, respectively. The reason for the higher resonance frequency is the extra inductance

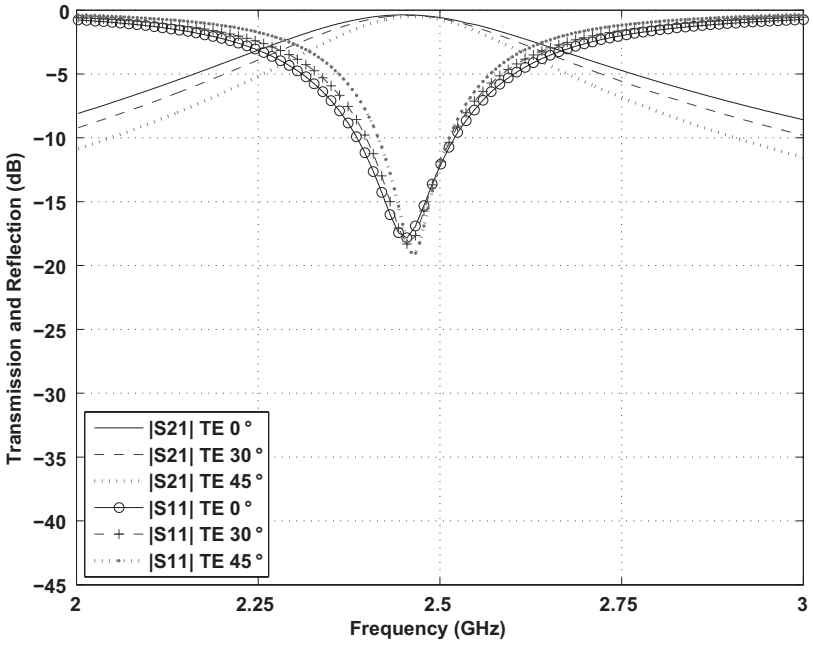

Figure 4.21 Theoretical transmission and reflection characteristics of the active circular FSS when the diodes are in the OFF state.

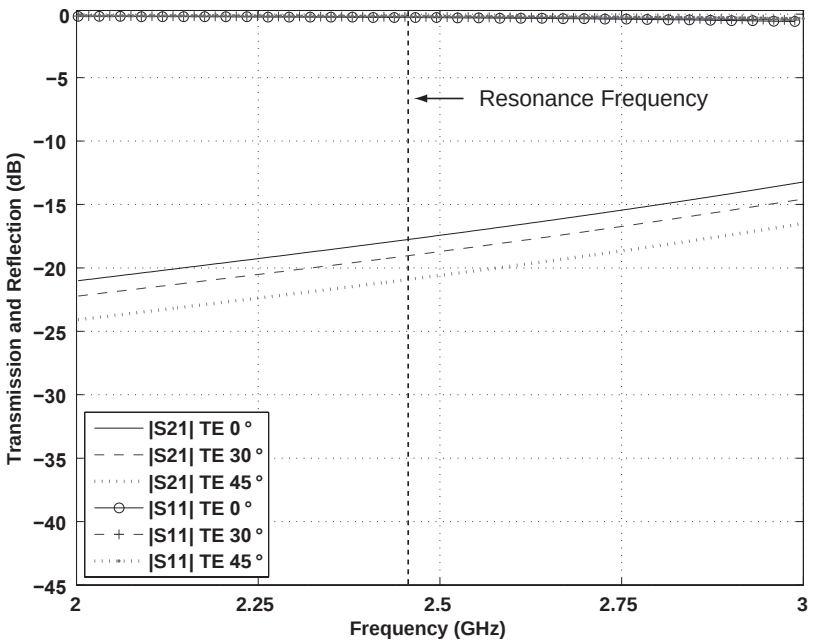

Figure 4.22 Theoretical transmission and reflection characteristics of the active circular FSS when the diodes are in the ON state.

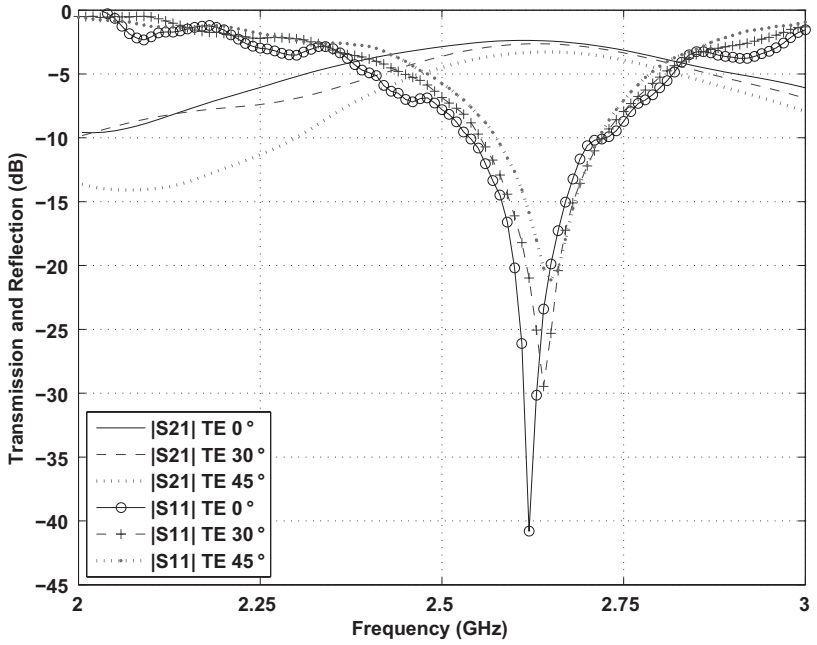

Figure 4.23 Measured transmission and reflection characteristics of the active circular FSS when the diodes are in the OFF state.

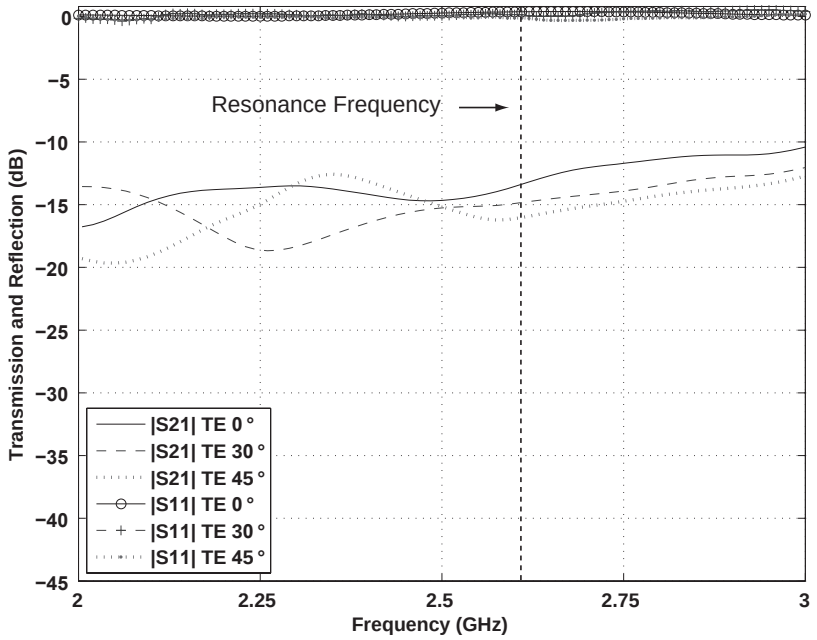

Figure 4.24 Measured transmission and reflection characteristics of the active circular FSS when the diodes are in the ON state.

contributed by the connecting DC lines at the end of the FSS prototype. Fig. 4.24 depicts the measured transmission and reflection coefficients for TE incidence when the diodes are in the ON state. For 0°, 30°, and 45° incidence angles, the reflection coefficient is almost 0 dB while the transmission loss is 13.1, 14.8, and 15.8 dB, respectively. Therefore, at 0°, 30°, and 45° angles of incidence, the transmission loss can be varied by 10.4, 12, and 12.4 dB, respectively, by switching the PIN diodes from OFF to the ON state.

The square-loop active FSS has a clear practical advantage over the circular-loop FSS due to its angle of incidence stability for both TE and TM polarisations. Also, it is stable up to a 60° angle of incidence in contrast to the 45° in the circular-aperture FSS case. However, for TE polarisation, the theoretical and measured transmission losses for both FSSs are almost the same for normal and oblique incidence. The additional average transmission loss for the square-loop FSS is 10 dB while it is 12 dB for circular-aperture FSS.

4.10 Production Cost

The square loop single layer active FSS prototype was fabricated using 1500 diodes with 375 FSS elements (4 diodes per unit cell). The price of the single diode used in FSS modeling and fabrication is about AUD 0.30. Therefore, for 1500 diodes the price becomes AUD 450 (plus the FSS fabrication cost). For practically large FSS prototypes, the cost may increase further due to use of more diodes and development of dc power supply. However, the cost may be reduced by using techniques as described in [110].

The use of any FSS design to control wireless coverage in a building environment depends on many factors, such as transmitting source power, receiver sensitivity,

room layout, distance between sources and building construction materials. It is not proposed that entire rooms be coated with FSS. This is discussed in [100] in which a simple path loss analysis shows that > 30 dB transmission loss may be required for an FSS wall, which these FSSs designs would not provide. The potential in FSS designs is in the use as a small aperture embedded in a shielded room, as discussed and demonstrated in [100]. In this case and with full recognition of the factors mentioned above, FSSs designs presented in this chapter offer a practical solution.

4.11 Conclusion

In this chapter, the theoretical and experimental results for two single-layer switchable FSSs are presented. PIN diodes along with square or circular-apertures are used. The FSS with square-loop apertures has shown a stable transmission response for both TE and TM polarisations up to 60°, while the FSS with circular loop apertures is not stable for TM polarisation (and angles higher than 45°). For square-loop aperture FSS, an average additional measured transmission loss of 10 dB is achieved for both polarisations at normal and oblique incidence, by switching PIN diodes between reverse and forward bias. Further isolation may be obtained by using a dielectric with a lower loss tangent and better-quality PIN diodes. Besides other wireless applications, it may find use in electronically reconfiguring the electromagnetic architecture of buildings.

Chapter 5

Energy-Saving Glass Characterisation

In this chapter, measurement techniques for the relative permittivity and conductivity of the glass are presented, while the electrical properties of metal-oxide layers as used in glass manufacturing are also discussed. Furthermore, the normal and oblique incidence transmission characteristics of one of the energy-efficient glass panels, at microwave frequencies for both parallel (TM) and perpendicular (TE) polarisations, are presented. The Optitherm^{TM}SN, manufactured by Pilkington [113], has about 30 dB average attenuation to signals in the 800 MHz to 6 GHz frequency band. Both theoretical and measured results indicate that the attenuation increases at oblique angles for perpendicular (TE) polarisation, while it decreases in the case of parallel (TM) polarisation.

The research presented in this chapter has been published as shown below:

Conference Papers

1. **Ghaffer I. Kiani**, Anders Karlsson, Lars Olsson, and Karu P. Esselle, "*Transmission Analysis of Energy Saving Glass Windows for the Purpose of Providing*

FSS Solutions at Microwave Frequencies", IEEE Antennas and Propagation Society International Symposium, San Diego, California, USA, 5-11 July 2008, Page(s): 1-4.

2. **Ghaffer I. Kiani**, Anders Karlsson, Lars Olsson, and Karu P. Esselle, "*Glass Characterization for Designing Frequency Selective Surfaces to improve transmission through energy saving glass windows*", Asia Pacific Microwave Conference (APMC), Bangkok, December, 2007.

5.1 Measurement of Relative Permittivity and Conductivity of Glass

In this section, two different methods are presented to measure the relative permittivity and the conductivity of glass. The first method uses a parallel-plate capacitance measurement using a wheatstone bridge, in which the relative permittivity and conductivity are obtained only at lower frequencies. The second method uses a waveguide measurement to determine both permittivity and conductivity in an X-band waveguide. Both methods are described here.

5.1.1 Parallel-Plate Capacitor Method

The permittivity and loss tangent of float glass were measured using this classical method for reference. A Rohde & Schwarz VKB 3250 Dielectric Test Bridge with the KMT 5411 Guard Ring Capacitor were connected with a low-frequency generator as the signal source and an oscilloscope as the detector [114]. This allowed measurements of both permittivity and loss tangent at 1 KHz and 10 KHz. The measurement setup is shown in Fig. 5.1.

Figure 5.1 Photograph showing the setup of the parallel-plate guard-ring capacitor measurement method.

First the capacitance and loss tangent were measured with the glass as dielectric. Then the glass was removed and the measurements were made again. The relative permittivity was then calculated by using the equation:

$$\epsilon_r = \frac{C_{glass}}{C_{air}}$$

The procedure was repeated twice at both frequencies and the mean values of the results were obtained. For frequencies less than 10 KHz the measurements gave an average permittivity of 6.9 ± 0.05 and the upper bound for the conductivity was 10^{-4} S/m. Since the conductivity is very low and the relative error in conducting measurements is quite large as compared to the permittivity measurements, only an upper bound was found.

5.1.2 Waveguide Technique

A waveguide technique [114] was used to measure the permittivity and conductivity at high frequencies. The details are given in the Apendix. The measurements in the X-band gave $\varepsilon_r = 6.9 \pm 0.15$ and $\sigma < 5 \times 10^{-4}$ S/m. It is possible to reduce the errors in these measurements by manufacturing even better shaped samples. The conductivity of glass is very small and hence the relative error in its measured value is quite high. The permittivity was approximately constant in the frequency band.

The measured values of the permittivity at X-band frequencies coincide with those at $f \leq 10$ KHz. In both of these frequency bands, the measured conductivity is very small. From these observations the assumption is made that the permittivity is constant and that the conductivity is very small for all frequencies less than 10 GHz. This is in accordance with the frequency dependence of ε_r and σ for most insulating solid materials.

5.2 Coating Properties

There are two main types of coatings used in low-emittance (low-e) glass panels to provide thermal isolation, namely a hard coating and a soft coating. In hard-coating a very durable pyrolytic coating is sprayed at a high temperature on to the glass surface during the float-glass process. This coating is relatively durable and allows ease of handling and tempering. On the other hand, the soft or sputter coating utilises a technique in which very thin metal-oxide layers are deposited on the glass surface in a vacuum chamber to provide high infrared attenuation. This configuration is shown in Fig. 5.2 in which four very thin layers of the order of nanometres thick are applied to float-glass to provide high infrared attenuation. This technique provides a more expensive but high-performance alternative to the hard-coat glass.

In this chapter a soft-coat low-emittance glass manufactured by Pilkington [113] is presented. Pilkington Optitherm^{TM}SN [115] glass panels are very popular for providing high infrared attenuation. It has three very thin metal-oxide coatings with a silver layer sandwiched between them. In order to design an aperture-type FSS for this coating to achieve improved transmission through a glass panel, the electrical properties of the coating must be known. Due to commercial confidentiality, it is not possible to provide any further details about the properties of the layers. In this case, all four layers have been modelled as a combined surface impedance of 4 Ω per square. This value of surface impedance has been provided by Pilkington [113].

5.3 Transmission Analysis of Energy-Saving Glass

In this section the normal and oblique incidence transmission characteristics of one of the energy-efficient glasses panels are investigated at microwave frequencies. Both parallel (TM) and perpendicular (TE) polarisations are considered. The Optitherm ^{TM}SN [115], manufactured by Pilkington [113], has about 30 dB of average attenuation to signals in the 800 MHz to 6 GHz frequency band. The attenuation increases at oblique angles for perpendicular (TE) polarisation while it decreases in the case of parallel (TM) polarisation. As described earlier, frequency selective surfaces can be etched on the coated side of energy-saving glass to provide a bandpass solution at microwave frequencies while keeping infrared attenuation intact [89]. Therefore, it was necessary to analyse the transmission properties of windows before devising a practical FSS solution. Pilkington, located in Sweden, provided us with different samples of glass panels. Theoretical and measured results for Pilkington Optitherm^{TM}SN glass [115] are presented here.

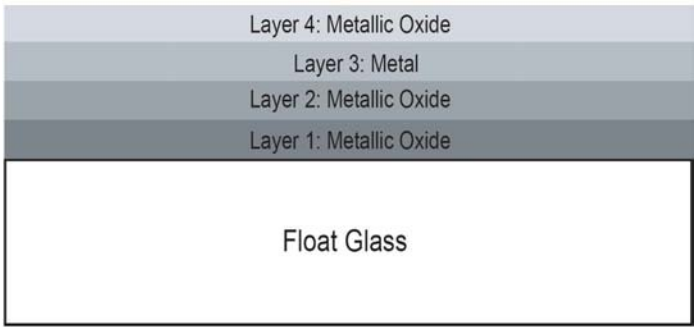

Figure 5.2 A typical arrangement of the soft-coat layers on the float glass.

5.4 Simulation

The theoretical results are obtained by using periodic boundary conditions in CST Microwave Studio (Frequency-Domain Solver). The length and the width of the unit cell employed in the simulation is 20 mm (see Fig. 5.3). The thickness of the glass substrate is 3.82 mm. Its relative permittivity is 6.9 and its conductivity is 5×10^{-4} S/m. The coating is modelled as a resistive sheet with 4 Ω / square.

5.5 Measurement Setup

The transmission measurement setup is shown in Fig. 5.4. HyperLog 7060 log-periodic antennas from the Aariona company, having a frequency range of 700 MHz to 6 GHz, were used for transmission measurements [9]. It was observed that there was no major difference between the measured data obtained in an anechoic chamber and those obtained in a free-space environment. Therefore, the measurements were carried out in free space and the glass panel was kept in the far field of the antennas. The distance between the two antennas (200 mm approx. between tips) allowed measurements up to a 60° angle of incidence. The antennas were connected to a network analyser (Rohde & Schwarz ZVC, 20 KHz to 8 GHz). The setup was calibrated in free

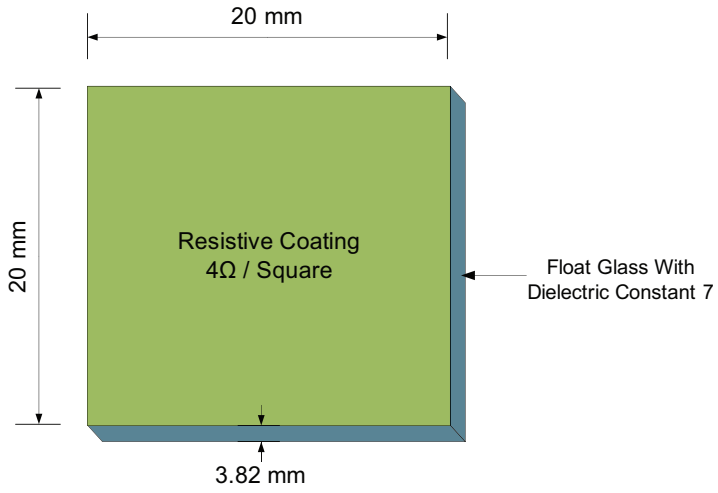

Figure 5.3 The unit cell employed for simulation.

space and hence 0 dB value corresponds to that. The size of the glass panel is about 1.9 m by 1.1 m, and it was kept on the floor during the measurement process to avoid any leakage under the window. A large glass panel was used for the measurement to reduce edge effects, though it was difficult to handle. The results obtained from this setup are in good agreement with the theoretical results.

5.6 Results

5.6.1 Perpendicular (TE) Polarisation

Theoretical Results

Figure 5.5 shows the theoretical transmission results for perpendicular (TE) polarisation from 0° to 60° angles of incidence. At 0°, the transmission losses at 900 MHz, 1800 MHz, 2.45 GHz and 5.25 GHz are 33.5 dB, 33.1 dB, 32.6 dB and 28.7 dB, respectively. The loss increases as the angle of incidence is increased from 0° to 60°.

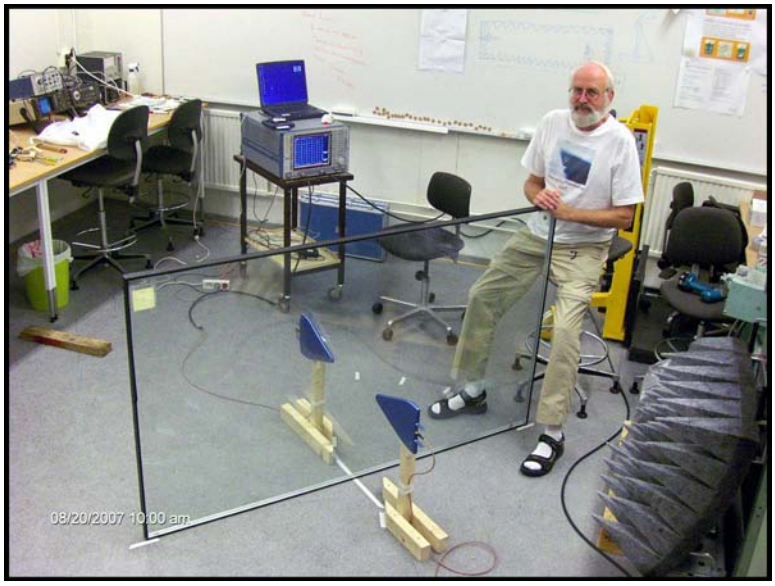

Figure 5.4 The measurement setup with Professor Lars Olsson holding the glass window between the log-periodic antennas.

Measured Results

Figure 5.6 shows the measured results at 0°. The transmission losses for the same frequencies are 30.8 dB, 31.5 dB, 31.6 dB and 28.1 dB, respectively. The loss increases with the increase in incidence angle in this case as well. It can be seen that there is a good agreement between theoretical and measured results.

5.6.2 Parallel (TM) Polarisation

Theoretical Results

Figure 5.7 shows the theoretical transmission results for parallel (TM) polarisation for the same range of angles. At 0° incidence angle, the transmission loss is same as in the case of perpendicular (TE) polarisation. However, due to Brewster effect, the transmission loss decreases with the increase in incidence angle.

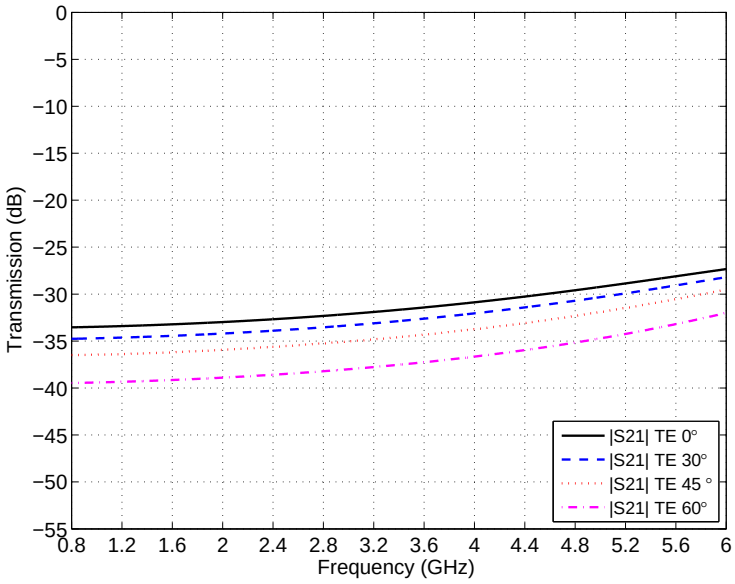

Figure 5.5 Theoretical transmission response of Optitherm^{TM}SN for perpendicular (TE) polarisation.

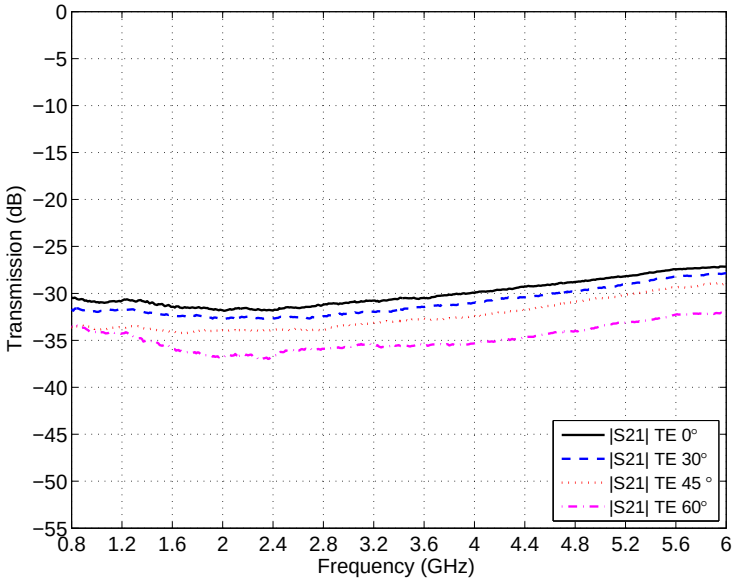

Figure 5.6 Measured transmission response of Optitherm^{TM}SN for perpendicular (TE) polarisation.

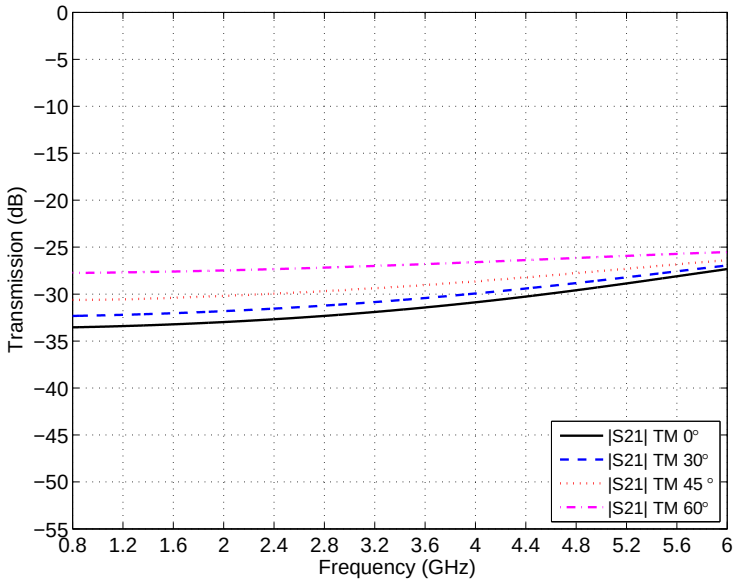

Figure 5.7 Theoretical transmission response of Optitherm^{TM}SN for parallel (TM) polarisation.

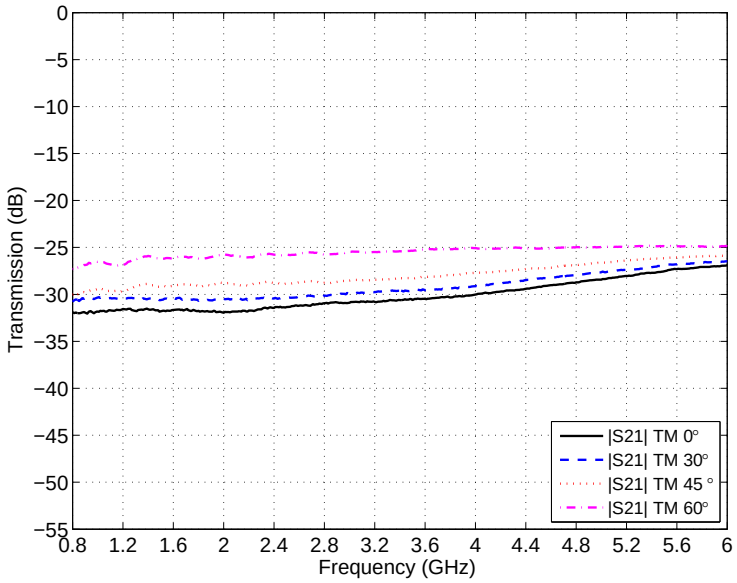

Figure 5.8 Measured transmission response of Optitherm^{TM}SN for parallel (TM) polarisation.

Measured Results

In Fig. 5.8 the measured transmission losses for the considered frequencies are 31.9 dB, 31.7 dB, 31.3 dB and 27.9 dB, respectively. The slight difference in the transmission loss between theoretical and measured results is due to the orientation of the antennas, which were fixed on wooden stands but still were able to move slightly. The transmission loss in this case also decreases with the increase in the angle of incidence (due to the Brewster effect).

5.7 Conclusion

In this chapter, the characterisation of commercially available glass panels is reported. It presents the measurement of relative permittivity and conductivity of glass using two different methods. It has been observed that both methods lead to very similar results. These values are very important for the design of an FSS on glass as described in Chapter 6. A typical description of Pilkington Optitherm^{TM}SN glass is given. For Optitherm^{TM}SN, about 30 dB of average transmission loss is observed over a frequency band of 800 MHz to 6 GHz for both TE and TM polarisations at normal incidence. This loss provides good security for WLANs operating at 2.45 GHz and 5.25 GHz but leads to poor transmission for mobile and personal communication systems. A bandpass FSS can provide a solution to this problem by improving the transmission of useful microwave signals while keeping good WLAN security and infrared attenuation, as illustrated in Chapter 6.

Chapter 6

Frequency Selective Surface Solution for Energy-Saving Glass

A bandpass FSS solution to the problem mentioned in Chapter 5 is proposed in this chapter. Since FSSs are spatial filters, the incoming wave may strike the FSS surface from any arbitrary angle and may have different polarisations. Therefore, any practical bandpass FSS design for this case should have a reasonably stable frequency response for waves having parallel (TM) or perpendicular (TE) polarisations incident either at normal or at oblique angles. A cross dipole is chosen as the FSS aperture due to its design simplicity and sufficiently stable transmission response. HP Suncool™ [116], an energy-saving glass from Pilkington [113], has been analysed for this purpose. Both theoretical and measured results show a reasonably stable frequency response and hence justify the usefulness of the FSS design.

Secondly, the variation in infrared (heat), visible (light) and microwave transmission through energy-saving glass due to etching of bandpass FSS is analysed. HP Suncool™and Optitherm™SN are investigated for the mentioned properties. Optitherm™SN (renamed as Optitherm™S4) [115] is an ultra-low emissivity, coated

glass offering good thermal isolation. The main effect of the low-emissivity coating is to reflect heat energy back into the building. The transparent coating also transmits heat from the sun (through light) and hence creates a naturally lit, comfortable working environment. Pilkington HP Suncool^{TM} [116] is also a superior solar control product with high visible-light transmittance and low-emissivity. The difference between HP Suncool^{TM}and Optitherm^{TM}SN is that the former passes less light to keep sun heat (coming through light) out of the building, keeping it cooler in summers. Therefore, Optitherm^{TM}SN has better performance in cold regions while HP Suncool^{TM}is better for hot regions. The difference in behavior between these products is achieved by changing the properties of the coating, which at microwave frequencies behaves as a resistive sheet having a finite value of surface resistivity.

The research presented in this chapter has been published or submitted for review, as shown below:

Journal Papers

1. **Ghaffer I. Kiani**, Anders Karlsson, Lars Olsson, and Karu P. Esselle, "*Transmission of Infrared and Visible Wavelengths Through Energy Saving Glass due to etching of Frequency Selective Surfaces*", IET Proceedings on Microwaves, Antennas and Propagation (Revised manuscript under review, 2009).

2. **Ghaffer I. Kiani**, Anders Karlsson, Lars Olsson, Martin Nilsson, and Karu P. Esselle, "*Cross-Dipole Bandpass Frequency Selective Surface for Energy Saving Glass Used in Buildings*", IEEE Transactions on Antennas and Propagation (Revised manuscript under review, 2009).

Conference Paper

1. **Ghaffer I. Kiani**, Anders Karlsson, Lars Olsson, Karu P. Esselle, and Martin Nilsson, "*Transmission Improvement of Useful Signals through Energy Saving*

Glass windows using Frequency Selective Surfaces", Workshop on Applications of Radio Science (WARS) Conference, Gold Coast, Queensland, Australia, 10-12 February, 2008 **(Won Best Paper Prize)**.

6.1 FSS Modelling

Figure 6.1 shows the unit cell of the cross-dipole bandpass FSS designed for HP Suncool^{TM}. CST Microwave Studio commercial software (frequency-domain solver) is used for simulation. The periodicity of the unit cell is 100 mm in both horizontal and vertical directions. The length and the width of each segment of the cross-dipole aperture are 64 mm and 8 mm, respectively. The FSS periodic structure is tuned to 1.3 GHz. This centre frequency is chosen in such a way that the transmission response of bandpass FSS does not appreciably improves the transmission at 2.45 GHz. The thickness of the glass is 6 mm while the relative permittivity is 6.9. The conductivity in the glass is 5 $\times 10^{-4}$ S/m as described in Chapter 5. The surface resistivity of the coating is 6 Ω per square. The value of surface resistivity is provided by Pilkington without details of the metal-oxide layer, due to commercial confidentiality.

First, the unit cell shown in Fig. 6.1 was analysed with a full coating (without FSS). The coating is modelled as an impedance boundary condition in CST Microwave Studio. The simulation is carried out from 800 MHz to 6 GHz using the frequency-domain solver, to obtain the effect of coating in the desired band (800-2200 MHz) as well as for WLAN bands (2.45 GHz and 5.25 GHz). This is due to the fact that in most of the cases it is desirable to attenuate WLAN signals, while allowing the passage of mobile telephone signals, GPS and personal communication signals through the FSS (as described in Chapter 3). Next, the cross-dipole FSS aperture is removed from the coated side of the unit cell as shown in Fig. 6.1. The results are presented in

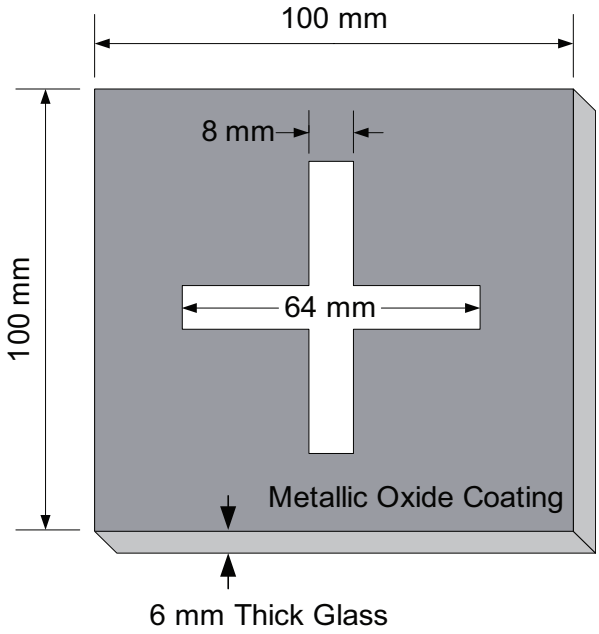

Figure 6.1 The dimensions of a unit cell of the cross-dipole frequency selective surface.

Section 6.6 for different polarisations and angles of incidence up to 45°. It can be noticed that the frequency response of this FSS is reasonably stable for the angles of incidence and polarisations considered.

6.2 Selection of FSS Element

The choice of an FSS element is mostly based on the need for good bandwidth and angular stability with respect to TE and TM polarisations. The cross-dipole FSS provided the required bandwidth and acceptable angular stability. Therefore, it was chosen for the FSS design due to its simplicity and relatively good performance. Also, it was noted that, due to the resistive nature of the coating, the angular stability was less affected as compared to a perfect electric conductor (PEC) surface. Had the coating been a PEC, the use of loop-type FSS elements may have been required for high bandwidth and better angular stability. However, in our research, the use

of a cross-dipole FSS yielded the required results and proved easier to etch than any complex FSS element. The reason was that the milling machines use standard tools to etch ordinary Printed Circuit Boards (PCBs) with copper. However, glass is more fragile than copper and it was quite difficult to etch complex FSS elements on to it (tools were not able to handle the bends and tend to break). However, even if the fabrication was possible, there was no need to design a complex FSS as a simple cross-dipole provided the desired results. Moreover, the use of low-pass FSS for transmission improvement has also been considered, however, a resonating cross-dipole FSS produced better results.

6.3 Measurement Setup

Figure 6.2 shows the measurement setup for glass with the FSS etched on the coated side of the glass sample. The setup was same as discussed in Section 5.5. A LPKF Protomat 95S/II milling machine from LPKF (Laser and Electronics) was used for etching [117]. The milling process is shown in Fig. 6.3.

6.4 Finite 2×2 Cross-Dipole FSS

One of the main challenges of the bandpass frequency selective solution for energy-saving glass is to maintain thermal isolation, while providing improved transmission in the useful RF/microwave bands. One solution which keeps IR transmission relatively low is to etch the FSS on only part of the energy-saving glass panel. This process is simpler and may cost less as opposed to etching the full glass sample during both pre- and post-manufacturing processes (as described earlier). To analyse this concept, a finite array of 2×2 cross-dipole FSS was etched on part of a glass sample having a

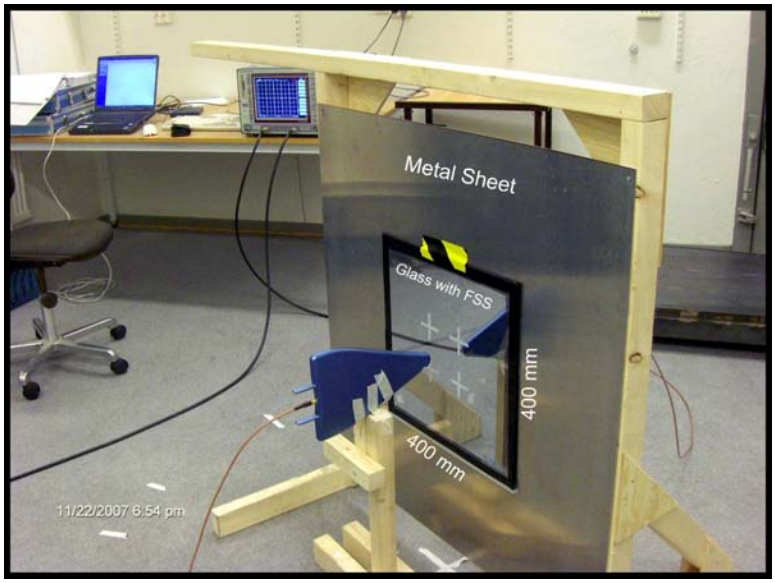

Figure 6.2 The measurement setup showing 2×2 cross-dipole FSS etched on part of a glass sample fixed in a metallic window between two log-periodic antennas.

length and a width of 400 mm, removing only 2.4% of coating. In such cases, the improvement in microwave transmission is uniform near the FSS area but may not be uniform over the whole panel area. For measurement purposes, the angle of incidence was defined at the centre of the array. However, to find the practical benefit of this concept, an FSS should be etched on a part of a larger glass sample, and transmission needs to be measured in various locations in a more practical building environment.

6.5 Fabrication Issues

It can be noticed in Fig. 6.2 that, due to the etching of the FSS pattern on the coated side of the energy-saving glass, the aesthetic appearance of the glass is severely degraded. Therefore, a cross-dipole FSS with a 64 mm thickness may not seem to be practical if fabricated through a milling process. This is due to the fact that the milling tool also cuts into the glass (not just the coated surface) due to the very

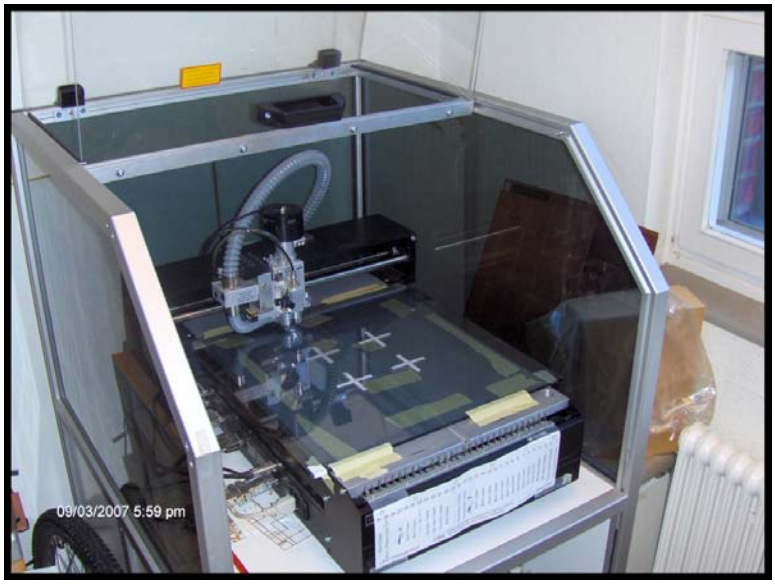

Figure 6.3 Milling process of etching cross-dipole FSS on the coated side of a glass sample.

small thickness of coating. Also, due to the non-PEC nature of the metal-oxide coating, it is very hard to achieve a strong resonance as described earlier. Therefore, the transmission of RF/microwave signals can only be improved to an acceptable level by increasing the width of the FSS unit cell. Therefore, for a practical FSS design with greater unit-cell width, two different aspects related to mass production of energy-saving glass (with an FSS solution) must be considered. These aspects include either pre-production or post-production application of the FSS filter on energy-saving glass. In the pre-production process, the FSS can be applied to the glass during the sputtering process. It can be done by applying an FSS mask pattern on the side of the glass that needs to be coated. The glass can then be passed through vacuum chambers where the oxide layer/s is/are deposited. Once the glass product is ready, the mask can be removed, leaving an aperture-type FSS pattern on the coated side of the energy-saving glass. The colour of the glass and the coating have to be same, so that the appearance of the final product will be least affected giving an acceptable

transparency. In the post-production process, the FSS can be applied on the coated side of the glass after the glass is manufactured (with coating). In this case, techniques like the use of laser beams or sand blasts (by applying an aperture-type mask on coated side) can be considered for the production process. In both the cases, the appearance of the glass will be least disturbed.

6.6 Results

6.6.1 TE Theoretical

Figure 6.4 shows the theoretical transmission through energy-saving glass for perpendicular (TE) polarisation. Let us first consider the results with a full coating. At 0°, 30° and 45° incidence angles, an average transmission loss of 30 dB, 31 dB and 33 dB can be observed in the useful frequency band, respectively. The transmission loss increases with an increase in incidence angle. For 2.45 GHz and 5.25 GHz WLAN bands, the attenuation at a 0° incidence angle is 28 dB and 24 dB, respectively. With the increase in incidence angle, the attenuation at 5.25 GHz remains almost unchanged. At 2.45 GHz, it rises to 29 dB and 31 dB for 30° and 45° incidence angles, respectively. As mentioned earlier, it is an added advantage of energy-saving glasses that they provide good WLAN confinement and security due to the IR attenuation; therefore it is recommended that, by etching an FSS, this property should not be degraded significantly.

Figure 6.4 also shows the transmission response of the cross-dipole FSS designed on the coated side of HP Suncool^{TM}. It should be noted that the dimensions of the unit-cell and the cross-dipole FSS have been selected in such a way that it resonates at 1.3 GHz. This resonance frequency is slightly less than the centre frequency of the band 800-2200 MHz, i.e. 1.5 GHz. As the coating is not a perfect electric conductor

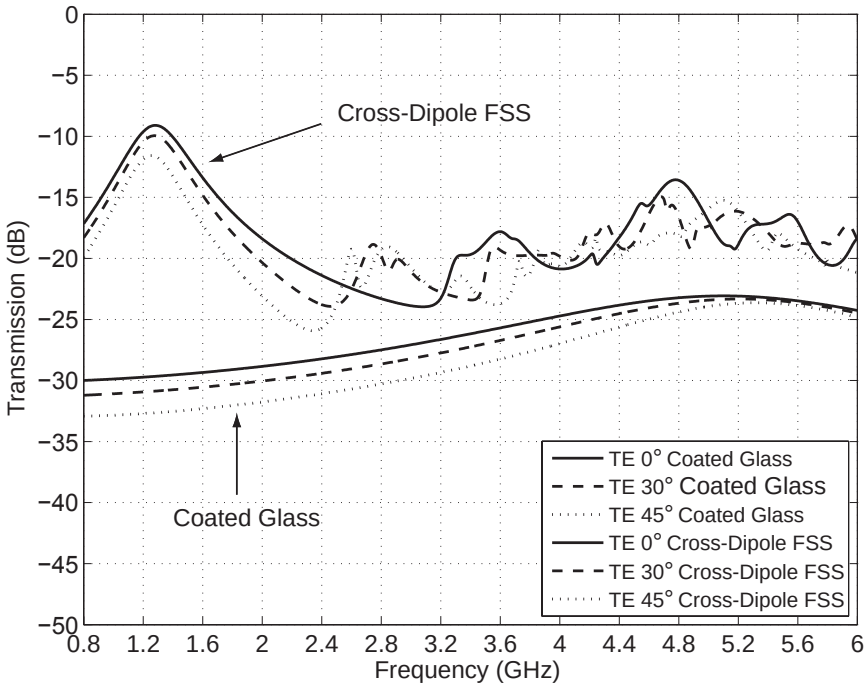

Figure 6.4 Theoretical TE transmission results of HP Suncool^{TM}with full coating and cross-dipole FSS designed on the coated side of the glass sample.

(PEC), it is difficult to obtain a sharp resonance. Therefore, it is intended that the transmission curve start to roll off before the limiting frequency (2.2 GHz) of the useful bandwidth to maintain a high transmission loss at 2.45 GHz.

At the resonance frequency of 1.3 GHz, the transmission loss at 0°, 30° and 45° incidence angles is 9 dB, 10 dB and 13 dB, respectively. Therefore the transmission improvement at the resonance frequency is 21 dB, 21 dB and 20 dB, respectively. On average, about 15 dB of transmission improvement is achieved in the useful frequency band for normal incidence. Due to the FSS, there is also an increase in transmission in the WLAN bands. On average, about 6 dB and 5 dB of increase in transmission is noticed at 2.45 GHz and 5.25 GHz, respectively. For an FSS on a resistive coating (not a PEC), these results are very encouraging and hence the WLAN security is maintained at a very reasonable level while the transmission improvement in the

useful frequency band is quite good.

Another important aspect of FSS design for such energy-saving glass is the degradation in IR attenuation as a result of etching the FSS in the coating. A linear relationship can be approximated because the percentage decrease in the IR attenuation is directly proportional to the percentage of area removed by the FSS elements. This important aspect is discussed in Section 6.8.

6.6.2 TE Measured

Figure 6.5 shows the measured results for perpendicular (TE) polarisation. For glass covered with a full coating, an average transmission loss of 26.7 dB, 27.9 dB and 30 dB can be observed at 0°, 30° and 45° incidence angles, in the useful frequency band, respectively. The transmission loss in this case is slightly less than the theoretical results due to diffraction from the edges of the measurement setup. For the 2.45 GHz and 5.25 GHz WLAN bands, the attenuation at 0° incidence angle is 24.9 dB and 21 dB, respectively. With the increase in incidence angle, there is a slight change in transmission at 5.25 GHz while it is 26.5 dB and 27.8 dB for 2.45 GHz at 30° and 45°, respectively. In this case as well, the theoretical and measured results are in good agreement.

Figure 6.5 also shows the transmission response of the finite 2×2 cross-dipole FSS etched on the coated side of a HP Suncool^{TM}glass sample (shown in Fig. 6.2). The resonance is observed at about 1.4 GHz, which is close to the theoretical prediction. The comparison between the measured transmission for normal incidence and the corresponding theoretical result is very good in the desired band, especially close to the resonance frequency. Also, the measured frequency response of this finite FSS is reasonably stable with the angle of incidence, but not as stable as the theoretical results for the infinite FSS presented earlier. At the resonance frequency, the transmission

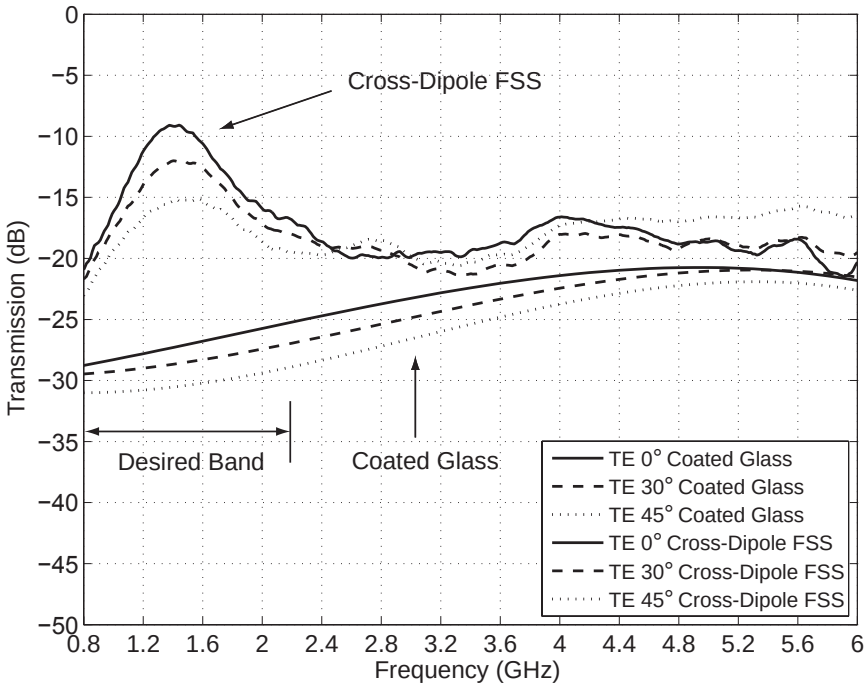

Figure 6.5 Measured TE transmission results of HP Suncool^{TM}with full coating and 2×2 cross-dipole FSS etched on the coated side of the glass sample.

loss at 0°, 30° and 45° incidence angles is 9 dB, 12 dB and 15.1 dB, respectively. Therefore the transmission improvement at the resonance frequency is 18.5 dB, 16.5 dB and 15.4 dB, respectively. On average, about 11.3 dB of transmission improvement is achieved in the desired band for normal incidence, compared with the 15 dB improvement in the theoretical results. Moreover, about 6 dB of average increase in transmission (for all angles considered) is noticed at 2.45 GHz. There is about 2 dB of increase in the transmission loss at 5.25 GHz. Therefore, the measured results are very encouraging for WLAN confinement and security.

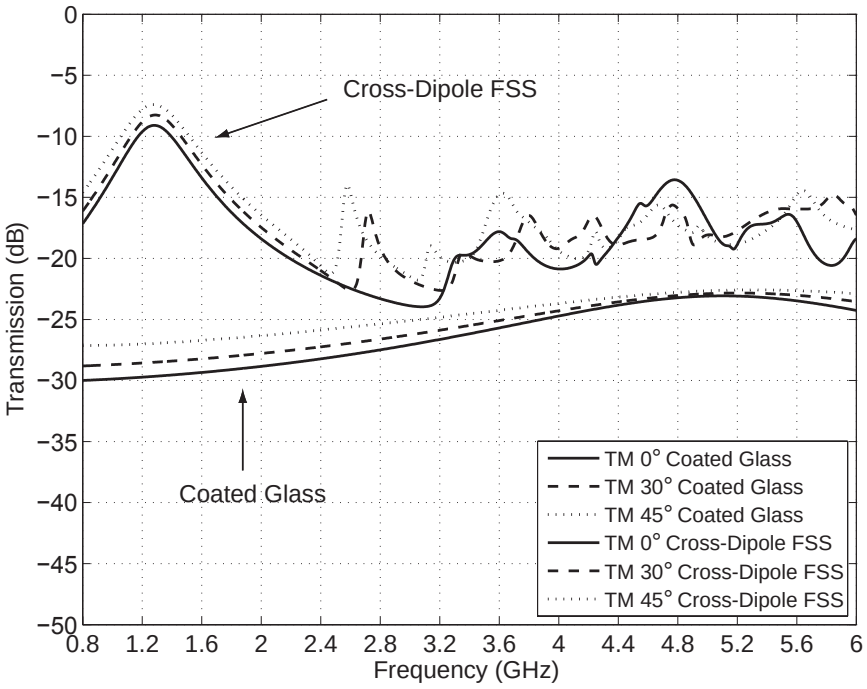

Figure 6.6 Theoretical TM transmission results of HP Suncool^{TM}with full coating and cross-dipole FSS designed on the coated side of the glass sample.

6.6.3 TM Theoretical

Figure 6.6 shows the theoretical results for parallel (TM) polarisation. With a full coating, an average transmission loss of 30 dB, 28 dB and 26 dB can be observed at 0°, 30° and 45° incidence angles in the useful frequency band, respectively. The transmission loss decreases with the increase in incidence angle due to the Brewster effect. For the 2.45 GHz and 5.25 GHz WLAN bands, the attenuation for normal incidence is 28 dB and 24 dB, respectively. With the increase in incidence angle, the attenuation at 5.25 GHz remains almost unchanged while it is 27.5 dB and 26 dB for 2.45 GHz at 30° and 45°, respectively.

The transmission response of the cross-dipole FSS for TM polarisation is also depicted in Fig. 6.6. At the resonance frequency of 1.3 GHz, the transmission loss at 0°, 30° and 45° incidence angles is 9 dB, 8 dB and 7 dB, respectively. In this case

the transmission improvement at the resonance frequency of 1.3 GHz is 21 dB, 21 dB and 20 dB, respectively (same as TE case). On average, about 15 dB of transmission improvement is achieved in the useful frequency band for normal incidence. In this case as well, there is an increase in transmission in the WLAN bands. On average, about 4 dB and 5 dB of increase in transmission is noticed at 2.45 GHz and 5.25 GHz, respectively. This is quite similar to the TE case. Therefore, this particular FSS design provides good transmission improvement in the useful frequency band while keeping a WLAN confined and secure.

6.6.4 TM Measured

Figure 6.7 shows the measured results for parallel (TM) polarisation. For coated glass, an average transmission loss of 26.7 dB, 25.5 dB and 24.6 dB is found at 0°, 30° and 45° incidence angles in the useful frequency band, respectively. The Brewster effect can be noticed in this case as well. For the 2.45 GHz and 5.25 GHz WLAN bands, the attenuation at a 0° incidence angle is 24.5 dB and 20.5 dB, respectively.

The transmission response of the cross-dipole FSS for TM polarisation is also depicted in Fig. 6.7. Again, the measured results for normal incidence compare well with the theoretical results for frequencies close to the resonance frequency. The resonance frequency for the TM case is 1.4 GHz and the transmission loss at resonance is about 9 dB. Unlike in the theoretical results, an increase in transmission with incidence angle is observed only for certain frequencies in the desired band. The transmission improvement at the resonance frequency of 1.4 GHz is 18.2 dB, 17.5 dB and 15.7 dB, respectively, for incidence angles of 0°, 30° and 45°. On average, about 11.3 dB transmission improvement is achieved in the desired band for normal incidence. Also, WLAN confinement and security are quite good in this case as well for both 2.45 GHz and 5 GHz WLAN bands.

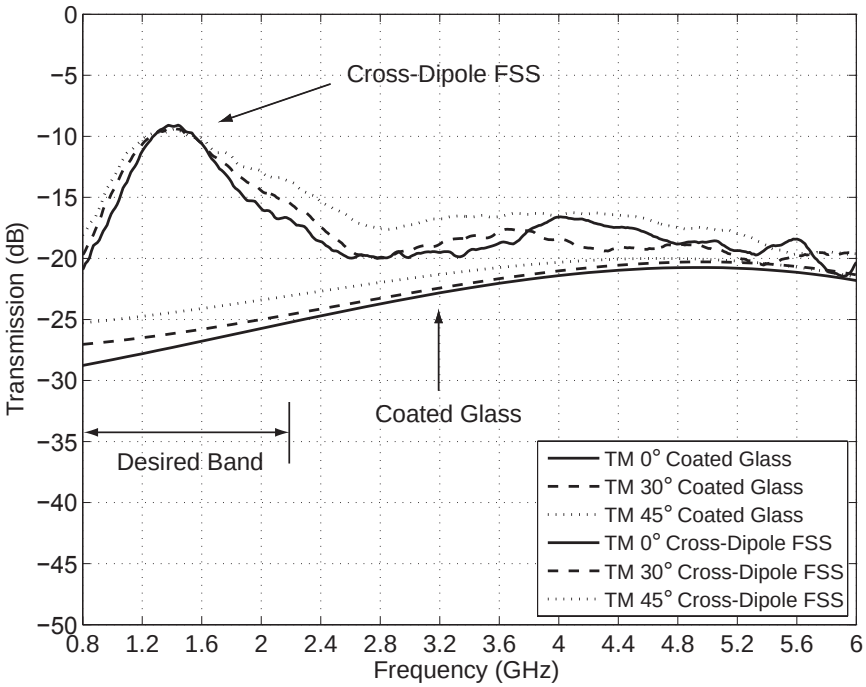

Figure 6.7 Measured TM transmission results of HP Suncool^{TM}with full coating and 2×2 cross-dipole FSS etched on the coated side of the glass sample.

6.7 Use of Low-Pass FSS for Transmission Improvement

This section describes a low-pass FSS design to improve the transmission of useful signals through energy-saving glass. Fig. 6.8 shows the unit cell of low-pass FSS modelled on the coated side of the glass. The dimensions of unit cell (substrate) is the same as in the cross-dipole case. The surface area removed from the unit cell is 9.75% (9.6% in cross-dipole FSS case).

CST Microwave Studio (frequency-domain solver) was used for simulating low-pass FSS, and the results are presented in Fig. 6.9. It can be seen that the FSS provides a very good transmission at low-frequencies, while it decreases with the increase in frequency, specially after 500 MHz. At 900 MHz, the transmission increase

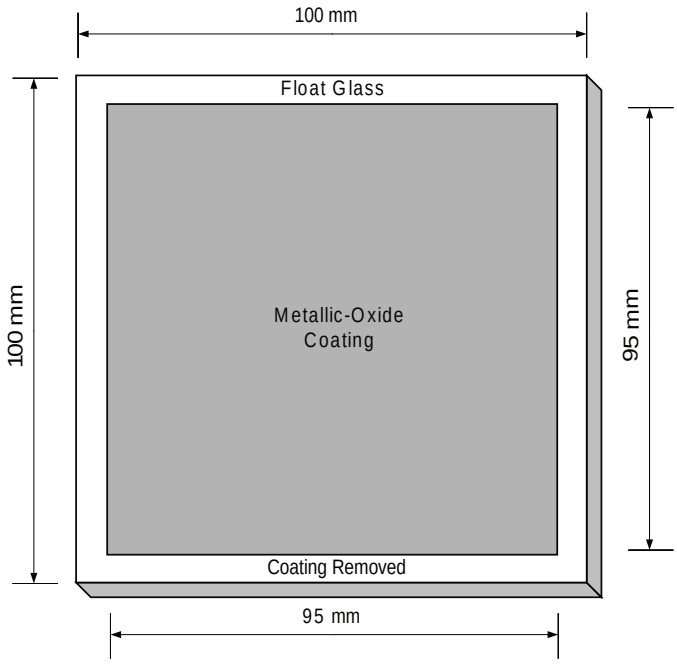

Figure 6.8 The dimensions of a unit cell of the low-pass frequency selective surface.

is 15 dB, while it is 5 dB at 2200 MHz. For cross-dipole case, the transmission increase is 18 dB and 8 dB respectively, however it is 21 dB at 1.3 GHz (resonance frequency). Therefore, a resonating FSS was preferred over a low-pass FSS, even when the difference is marginal. Also, a multi-band resonating FSS may also be considered for transmission improvement of particular frequency bands (please refer to the paper presented at WARS conference attached in the appendix).

6.8 IR and Light Transmission through Energy-Saving Glass due to FSS

In this section, the effect of etching of bandpass FSS apertures on infrared (heat), visible (light) and microwave transmission through energy-saving glass is investigated. In order to provide a good transmission solution for the useful RF/microwave frequency

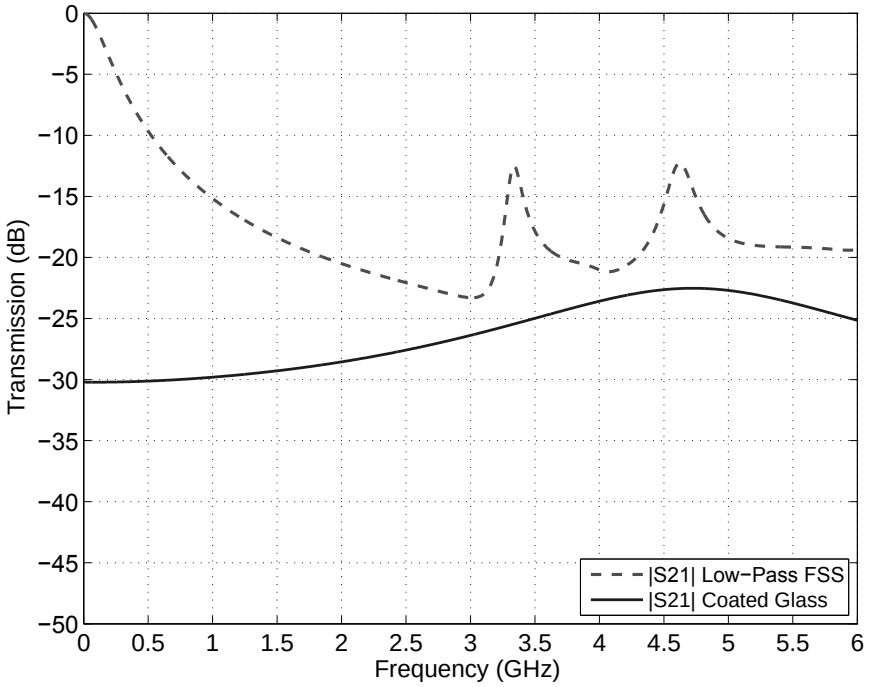

Figure 6.9 Theoretical transmission results of HP Suncool^{TM}with full coating and low-pass FSS designed on the coated side of the glass sample.

band, the etching of the FSS should not significantly degrade the IR attenuation property of the energy-saving glass. The experimental investigation described in Section 6.10 demonstrated that, for infrared wavelengths, a linear proportionality holds between the percentage area removed and the increase in transmission due to etching of rectangular apertures of different sizes (for both HP Suncool^{TM}and Optitherm^{TM}SN). For visible wavelengths, there is almost no change in transmission due to etching. This experimental study enables us to estimate the change in infrared and visible transmission when an FSS is etched in the coating. On the other hand, at microwave frequencies, the change in transmission is mainly determined by the resonance of the aperture, rather than the aperture area.

6.9 Measurement Setup for IR and Visible Light

Figure 6.10 shows the inner view of the PerkinElmer Lambda 900 UV/Visible/NIR (Near Field Infrared) spectrophotometer [118] with a glass sample. This spectrophotometer can only transmit signals through a small circular aperture with a diameter of 20 mm. Hence, it was impossible to measure a large glass sample with an FSS etched on the coated side. Therefore, firstly, an ordinary (float) glass sample with a length and a width of 100 mm was placed in front of the circular aperture to measure the transmission of infrared and visible wavelengths through it. The float glass response was recorded on a PC connected to the spectrophotometer and was taken as a reference. Secondly, one sample of each of HP Suncool^{TM}and Optitherm^{TM}SN having the same length and width as the float glass was placed in front of the circular aperture and the transmission was measured. Thirdly, a smaller rectangular aperture was etched in the coating of each sample and the measurement was repeated for the same wavelengths. Finally, this is repeated with a larger rectangular aperture. The configurations of the samples are shown in Figs 6.11 and 6.12.

6.10 Measured Results

6.10.1 Optitherm^{TM}SN

Figure 6.13 depicts the measured results for Optitherm^{TM}SN energy-saving glass for infrared and visible wavelengths. For reference, the result for float glass without coating is also depicted. It can be seen that, for the glass sample fully covered with a coating, about a 62% average decrease in infrared (1200 nm to 1700 nm) transmission has occurred while the response at visible wavelengths (400 nm to 700 nm) is almost unchanged. This means that the energy-saving glass is successfully attenuating in-

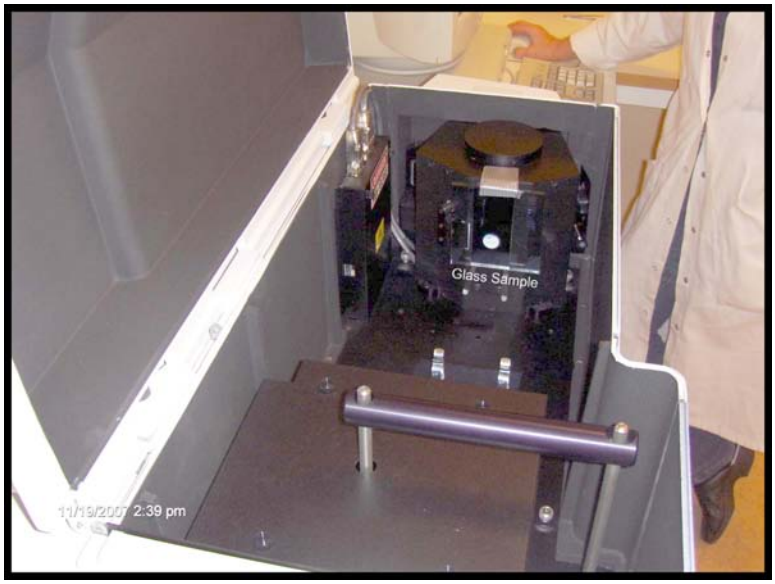

Figure 6.10 The inner view of the PerkinElmer Lambda 900 UV/Visible/NIR spectrophotometer with a glass sample.

frared (heat) while being transparent to visible light. When a rectangular 3 mm × 2.5 mm aperture (aperture 1), aligned to the center of the circular aperture in the measurement setup, was etched in the glass coating, the measurements show a small decrease in IR attenuation while the transmission of visible wavelengths is almost unchanged. When the same process was repeated with a larger 6.5 mm × 3.5 mm aperture (aperture 2), the results show a further decrease in IR attenuation. The relationship between the decrease in IR attenuation and the percentage area removed is discussed in Section 6.11.

6.10.2 HP Suncool ™

Figure 6.14 depicts the measured results for HP Suncool™energy-saving glass for infrared and visible wavelengths. The results for float glass without coating are also shown for comparison. As in the previous case, about 60% average decrease in infrared (1200 nm to 1700 nm) transmission has occurred as a result of the full coating. The

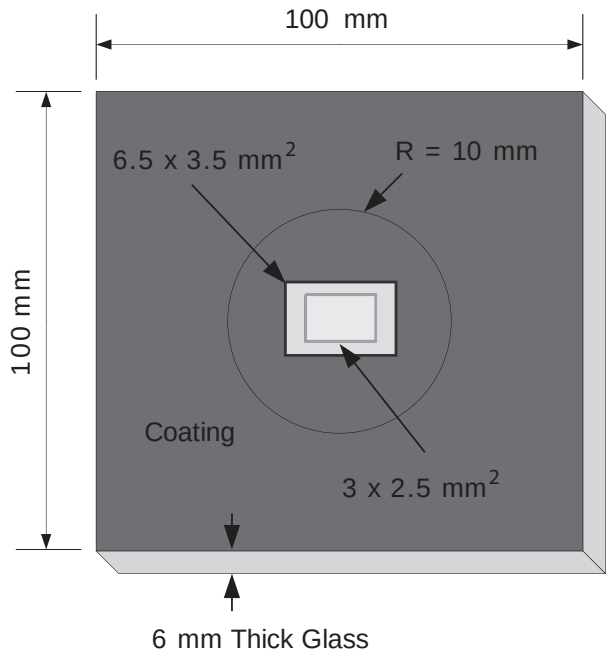

Figure 6.11 The sample of Pilkington Optitherm^{TM}SN, the circular measurement area and the dimensions of two rectangular apertures removed from the coating.

response at visible wavelengths (400 nm to 700 nm) is different in this case and there is about 35% average decrease in transmission. The purpose of this attenuation at visible wavelengths is to stop heat coming into the buildings through visible light. Therefore, heat in both (light and infrared) forms is attenuated in order to keep buildings cooler in hot regions. In order to analyse the effect of etching in this case, a 4 mm $\times$ 2.3 mm aperture (aperture 1) was etched in the glass coating such that it aligns with the centre of the circular aperture of the measurement setup. The measured result, also shown in Fig. 6.12, indicates a decrease in IR attenuation while the transmission of visible wavelengths is almost unchanged. The same process was repeated with a larger 6.9 mm $\times$ 3.5 mm aperture (aperture 2) and the results show a further decrease in IR attenuation.

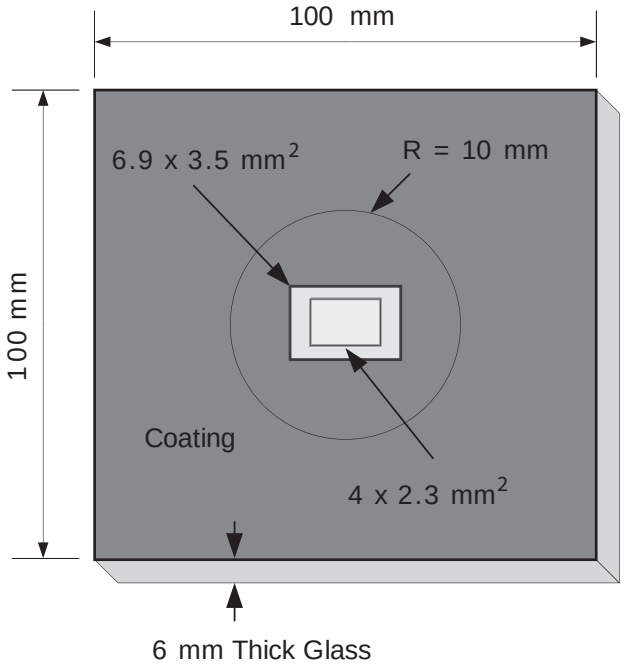

Figure 6.12 The sample of Pilkington HP Suncool^{TM}, the circular measurement area and the dimensions of two rectangular apertures removed from the coating.

6.11 Effect of Removal of Coating on Infrared and Visible Wavelengths

In this section the effect of etching the coating on the transmission of infrared and visible frequencies through energy-saving glass is discussed.

6.11.1 Optitherm^{TM}SN

In Fig. 6.15 the transmission of IR and visible waves is plotted against the percentage of area removed for Optitherm^{TM}SN. The wavelengths considered are 1200 nm, 1500 nm, 400 nm and 700 nm. From Fig. 6.9, the area of the circle is 314 mm^2, while the areas of aperture 1 (small) and aperture 2 (large) are 7.5 mm^2 and 22.75 mm^2, respectively. Therefore, these rectangular apertures take up 2.4% and 7.2% of the

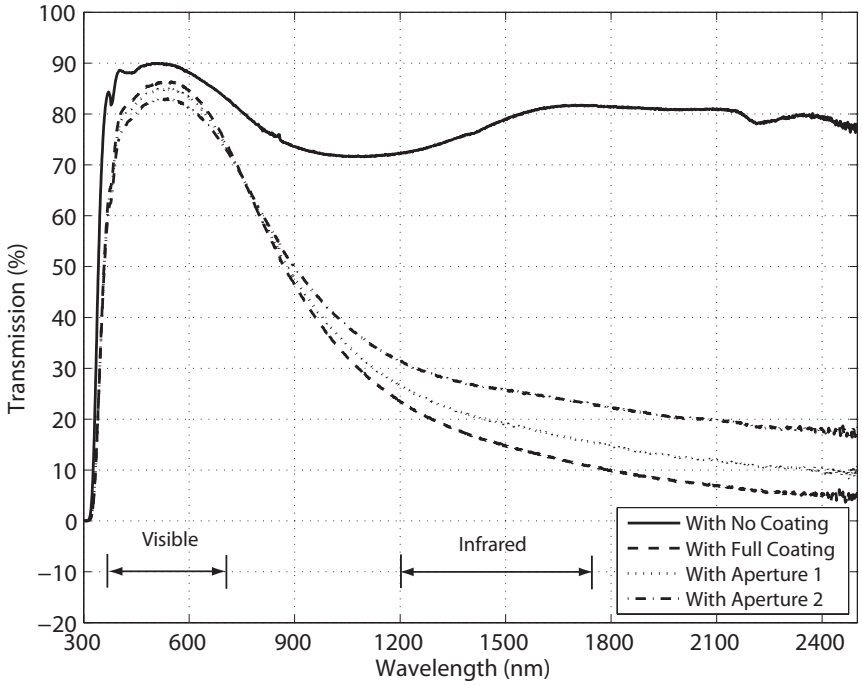

Figure 6.13 The response of Optitherm^{TM}SN glass with no coating, full coating, aperture 1 and aperture 2, at infrared and visible wavelengths.

circle area.

From Fig. 6.13, when the surface is not etched, the infrared transmission percentage at 1200 nm and 1500 nm wavelengths is 23.4% and 14.8%, respectively. For aperture 1, at the same wavelengths, the transmission percentage is 26.6% and 19.2%, while for aperture 2 these values are 31.4% and 25.7%, respectively. These changes in the infrared transmission percentage are plotted against the percentage area removed in Fig. 6.15. Included in this graph are also the results for a full coating. The small circles in the graph indicate data points. The graph is then extrapolated to a 10% etched area, for the FSS application discussed in Section 6.12. The same process was repeated for a 1500 nm wavelength and it can be seen that there exists a linear relationship between the transmission percentage and area removed.

Furthermore, to analyse the change in visible-light transmission with the removed

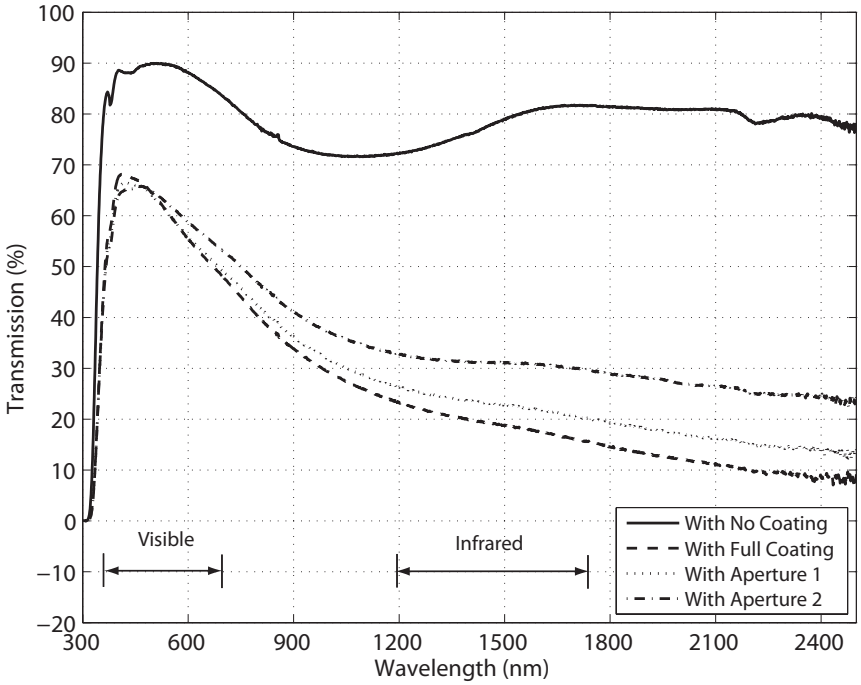

Figure 6.14 The response of HP Suncool^{TM}glass with no coating, full coating, aperture 1 and aperture 2, at infrared and visible wavelengths.

area, two extreme wavelengths of the visible spectrum band, i.e. 400 nm and 700 nm, are selected and it can be seen from Fig. 6.15 that at both wavelengths there is almost no change in the transmission. Moreover, for the glass fully covered with coating, the average transmission is about 77% for both visible wavelengths. This flow of sun heat coming with light into the buildings can keep buildings warmer in winter and hence Optitherm^{TM}SN is recommended for use in regions with a cool climate. High transmission at visible wavelengths also helps to improve the aesthetics and provides a good transparency.

6.11.2 HP Suncool ™

Figure 6.16 shows the corresponding results for HP Suncool^{TM}in terms of the percentage area removed to the change in the infrared and visible transmission. The

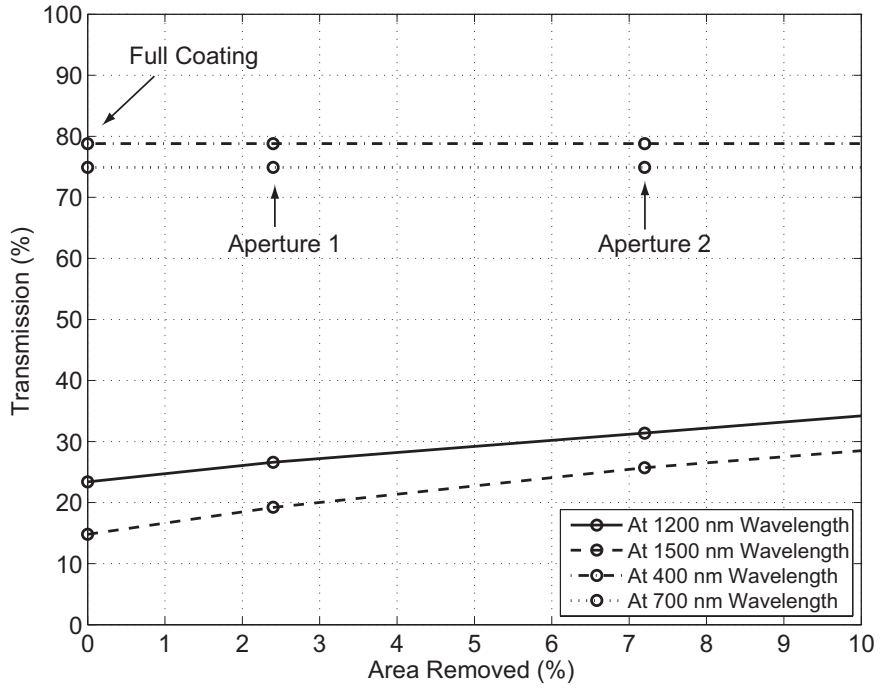

Figure 6.15 The effect of coating removed on the infrared and visible transmission for Optitherm^{TM}SN.

area of the circle is the same in this case (314 mm^2). Referring to Fig. 6.12, the areas of aperture 1 (small) and aperture 2 (large) are 9.2 mm^2 and 24.15 mm^2, and they take up 7.7% and 2.9% of the circle area, respectively. In this case as well, the change in infrared transmission is investigated at 1200 nm and 1500 nm wavelengths. For example, from Fig. 6.12, at 1200 nm wavelength, the transmission percentage with full coating, with aperture 1, and with aperture, 2 is 23.8%, 26.3% and 32.8%, respectively. Data for two IR wavelengths are plotted in Fig. 6.16 and it can be seen that there is again a linear relationship between the percentage area removed and the percentage infrared transmission.

Figure 6.16 also shows the change in transmission of visible wavelengths (400 nm and 700 nm) for HP Suncool^{TM}. The percentage areas removed in this case are the same as in the infrared case. The change is almost linear in this case as well for

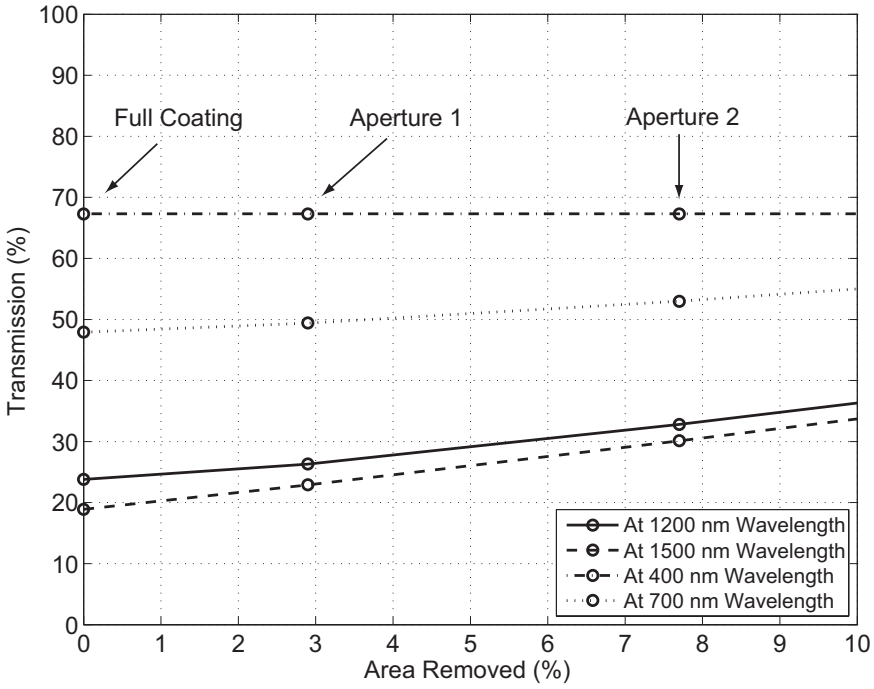

Figure 6.16 The effect of coating removed on the infrared and visible transmission for HP Suncool^{TM}.

both wavelengths and an average percentage transmission for the glass covered with coating is about 59%. As a result, HP Suncool^{TM}is more suited to regions with hot weather where it is also required to attenuate the heat from the sun coming into the buildings. This helps in keeping buildings cooler in summer while maintaining an acceptable transparency.

6.12 Effect of Etching an Aperture-Type Bandpass FSS

This section analyses the effect of removal of coating due to etching of a bandpass frequency selective surface. Cross-dipole aperture-type FSS designs are considered. First, both theoretically and experimentally, the desirable effect of increased transmis-

sion at microwave frequencies is investigated. Next, the undesirable effect of increased transmission of IR waves is estimated, by extrapolating experimental data presented in the previous section. Fig. 6.1 shows the unit cell of one aperture-type FSS etched in the coating of HP Suncool^{TM}. The thickness of the glass, its relative permittivity, conductivity and the surface resistivity are the same as described in Section 6.1. A greater inter-element spacing of cross dipoles is selected to achieve a narrow-band FSS response with a relatively sharp roll-off. Since the coating is not a perfect electric conductor (PEC), it is quite challenging to attain an ideal resonance.

6.12.1 RF/Microwave Theoretical Results

The unit cell shown in Fig. 6.1 was simulated with a full coating (without cross-dipole FSS) with properties described in Section 6.1. It can be seen in Fig. 6.17 that, due to the presence of the coating on the glass surface, there is an appreciable attenuation of useful RF/microwave signals (800-2200 MHz). On average, about 27 dB of attenuation occurs from 800 MHz to 6 GHz.

In the next step, a cross-dipole aperture (8 mm width) is removed from the coating of the unit cell and the simulation results are depicted in Fig. 6.17. The FSS resonates at 1.3 GHz, giving a peak transmission coefficient of -9 dB. About 20 dB of transmission improvement is predicted at 1.3 GHz while an average transmission improvement of about 15 dB is found in the useful RF/microwave frequency band. Also, there is an advantage with this design as the increase of transmission in the WLAN bands is small, which is desirable to maintain WLAN confinement and security. At 2.45 GHz the transmission is increased by only 5 dB while at 5.25 GHz it is 4 dB. Therefore, this design can be useful in practice where a confined and secure WLAN is a requirement. The percentage area removed from the unit cell due to the FSS is 9.6%.

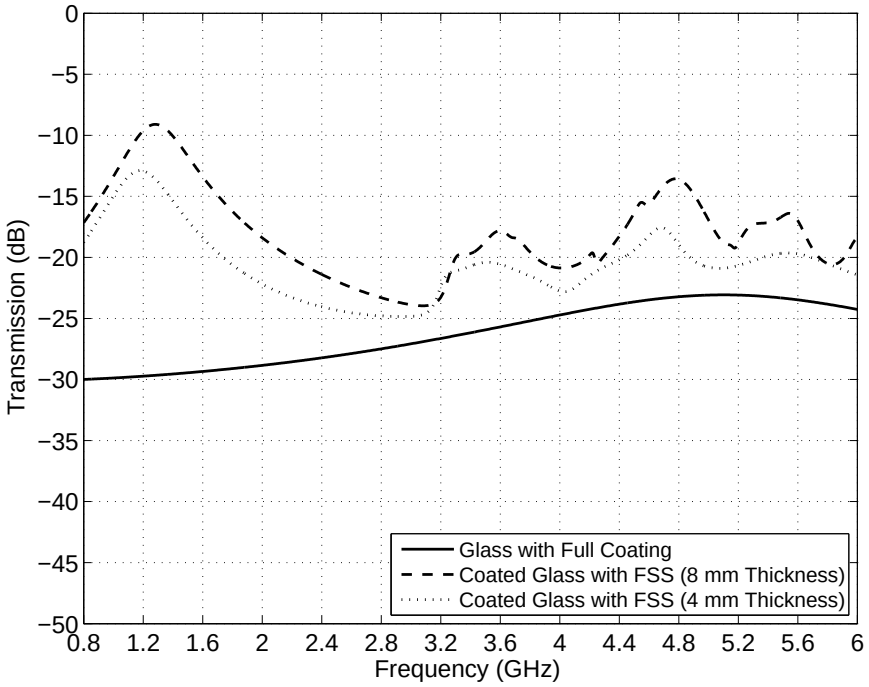

Figure 6.17 Theoretical transmission of HP Suncool^{TM}with full coating, with 8 mm and 4 mm cross-dipole FSSs etched in the coating.

Figure 6.17 also shows the theoretical transmission results for an aperture-type cross-dipole FSS with a smaller (4 mm) aperture width. In this case, the resonance frequency shifts slightly downwards and a reduction in peak transmission can also be noticed (compared to an FSS with an 8 mm aperture). The transmission improvement at resonance is about 16 dB while the average improvement in transmission is approximately 12 dB. At 2.45 GHz WLAN frequencies the transmission is increased by only 3.5 dB while at 5.25 GHz it is 2.5 dB. Therefore, the FSS with an 8 mm aperture is preferred for a practical design (over the 4 mm one) due to its better transmission improvement in the RF/microwave band. On the other hand, the 4 mm aperture causes less degradation of IR attenuation. Please note that the measured results for 8 mm aperture FSS are presented in Figs. 6.5 and 6.7, while only theoretical results for 4 mm aperture FSS are given in this section for comparison.

6.12.2 Effect at Infrared and Visible Wavelengths and Trade-Off

To make the 8 mm wide FSS, 9.6% of the coating has to be removed. The resulting undesirable decrease in the IR attenuation, due to this coating removal, can be estimated using graphs in Figs 6.15 and 6.16. From Fig. 6.16, for HP Suncool^{TM}, the resulting increase in IR transmission (at 1200 nm) is 10% (from 23.8% to 33.8%). At a 1500 nm IR wavelength, the increase is 12.1% (from 19.6% to 31.7%) . There is almost no change in visible-light transmission. This unwanted decrease in IR attenuation can be controlled by reducing the percentage of etching in the coating, but this also causes a reduction in the transmission of useful RF/microwave signals as discussed below.

In cases where such an increase in IR transmission is not acceptable, the 4 mm FSS design may be considered. In this case, only 4.96% of the coating is removed. From Fig. 6.16, the increase in IR transmission due to this FSS, at 1500 nm, is only 6.2% (from 23.8% to 30%). The cost is a decrease in RF/microwave transmission of 16 dB at the resonance frequency. In brief, a trade-off has to be made when designing an FSS to balance the improvement in RF/microwave transmission against the decrease in IR attenuation.

6.13 Production Cost

The cost of energy-saving glass with FSS solution may not be given in absolute terms at this stage of research, however, the process with which the FSS aperture is applied to the coated side may determine the cost of end product. For practical FSS design with greater unit cell thickness, two different aspects related to mass production of energy-saving glass (with FSS solution) can be considered. These aspects include

either pre-production or post-production of FSS filter on energy-saving glass.

In the pre-production process, the FSS may be applied on the glass during sputtering process. It can be done by applying an FSS mask pattern on the side of the glass that needs to be coated. The glass can then be passed through vacuum chambers where the oxide layers are deposited. Once the glass product is ready, the mask can then be removed, leaving aperture type FSS pattern on the coated side of energy saving glass. The colour of the glass and the coating has to be the same. Therefore, the aesthetic sense of the final product will not be affected much, giving a good see-through effect. This technique may require only one time investment in the glass production factory. However, the cost may still not be predicted at this early stage of the research.

In the post-production process, the FSS may be applied on the coated side of the glass after the glass is manufactured (with coating). In this case, the techniques like use of laser beams or sand blasts (by applying an aperture type mask on coated side and blasting with smooth sand particles) can be considered for the production process. In both the cases, the aesthetic of the glass will not be severely disturbed. However, in this case, the product cost may be more than the technique described earlier.

6.14 Conclusion

A solution to improve the transmission of RF/microwave signals through energy-saving glass is presented. It is achieved by designing and etching a cross-dipole bandpass FSS on the coated side of energy-saving glass. Besides the large increase in RF/microwave transmission, etching of an FSS in energy-saving glass also leads to an unwanted increase in IR transmission and associated heat transfer through

the apertures in the coating. It is required to keep the latter to a minimum level by etching as little coating as possible. In the infinite FSS presented here, 9.6% of the coating (by area) is removed in each unit cell. This will cause about the same percentage increase in the IR transmission.

As the energy-saving coating is made up of metallic oxide (which is not a good conductor), it is difficult to achieve a strong resonance or sharp roll-off. The FSS design used in this research can be customised to any frequency band in which a transmission improvement is required. It also provides good confinement and security in the 2.45 GHz and 5.25 GHz WLAN bands.

For two types of commercial energy-saving glass, the relationship between the transmission of infrared and visible waves and the percentage area etched has been established quantitatively. This relationship is crucial for providing a practical band-pass frequency selective surface (FSS) solution to improve the transmission of useful RF/microwave signals through energy-saving glass.

For approximately 20 dB of improvement of microwave transmission at 1.3 GHz through a glass panel, 9.6% of the coating area should be removed. This increases IR transmission by 10% (from 23.8% to 33.8%). A narrower (4 mm) FSS improves microwave transmission by 16 dB at the resonance frequency with a 6.2% increase in IR transmission. The area removed in this case is 4.96%. Therefore, in cases where a higher increase in IR transmission is not acceptable, a narrower FSS design may be considered.

Another way to reduce the increase in IR transmission is to etch the FSS on only a part of the energy-saving glass panel. This process is simpler and may cost less as opposed to etching on a full glass sample during manufacturing process. To analyse this concept, a finite array of 2×2 cross-dipole FSS was etched on part of a glass sample having a length and a width of 400 mm, by removing 2.4% of the coating. In

such cases, the improvement in microwave transmission is uniform near the FSS area but may not be uniform over the whole panel area. To find the practical benefit of this concept, an FSS should be etched on part of a larger glass sample and transmission needs to be measured in various locations in a more practical building environment.

Chapter 7

Conclusion

This thesis presents results of my investigations on the design of novel frequency selective surfaces that target specific applications in wireless communications. Three topics covered, namely FSS absorb/transmit filters, switchable FSS and FSS for energy-saving glass, each have the potential to dramatically improve the electromagnetic architecture of modern buildings and offices. For each topic, detailed measured results have been presented to confirm theoretical design data for obliquely incident waves with parallel and perpendicular polarisations. The research on FSS for energy-saving glass is multi-disciplinary in its approach as it considers IR and visible light properties as well as microwave performance. Based on the research presented in the thesis, this chapter highlights the outcomes and contributions that have been achieved in each of the three topics. After listing the contributions, the chapter concludes with suggestions for future research.

7.1 FSS Absorb/Transmit Filters

Two absorb/transmit FSS filter designs have been presented in Chapter 3. The first FSS design has good absorption characteristics for waves incident normally. This provides security and/or isolation for 5 GHz WLAN systems. It passes cellular phone signals and blocks 5 GHz signals by absorbing, as opposed to reflecting. However, its absorption performance is not stable when TE waves are incident at oblique angles (i.e. perpendicular polarisation). Hence, second FSS design was obtained and tested, achieving a stable frequency response for both polarisations in a more compact configuration. Here are the main contributions of this research:

- These are the first FSS spatial filter designs that stop propagation of specific bands by absorbing as opposed to reflecting, while passing other useful signals.

- Traditional FSS absorbers can only absorb a particular frequency band of interest, while transmission outside the band is attenuated. Moreover, Salisbury and Jaumman absorbers can absorb only certain frequencies while there is no transmission outside the band. However, this research showed that signals outside the stopband can also be transmitted while achieving good absorption in the stopband.

- The use of standard 377 Ω resistive sheet is common in previously designed absorbers. However, in this thesis a 50 Ω resistive sheet was used on one side of the dielectric material with a cross-dipole FSS. Different levels of absorption may be obtained by varying the value of the resistive sheet from 10 Ω to 300 Ω to provide more design flexibility. However, results for only 50 Ω are presented in this thesis. These dielectric materials with different surface resistivities are readily available from commercial suppliers.

- Another important aspect of absorber design is the distance between the ground plane and the resistive sheet. Previous designs used a standard $\lambda_0/4$ distance between the two layers of absorbers. However, in this design, the distance was successfully reduced to $\lambda_0/8$, making it more compact which is an important requirement at lower frequencies.

- This structure can help WLAN providers to: a) Stop people outside their premises from accessing the service; b) Increase service quality and speed by physically dividing the service area into several smaller areas and running independent WLANs in each small area, i.e., reusing channels; and c) By adding a second resistive FSS layer (in $\lambda_0/8$ design), the resulting triple-layer absorb/transmit filter can be incorporated in a wall of a building for advanced wireless security in such a way that its bi-directional absorbing characteristics can mislead an intruder (the total distance between the edges of the FSS absorb/transmit filter will still remain close to $\lambda_0/4$ as in the case of other conventional absorbers).

7.2 Switchable FSS

Two switchable bandpass FSS designs are presented in Chapter 4. The first design is a square-loop aperture type FSS while the other design is based on circular-loop aperture. It is experimentally demonstrated that almost 10 dB of additional transmission loss can be introduced on average, at the resonance frequency for both polarisations, by switching the PIN diodes to the ON state from the OFF state. The contributions from this Chapter can be summarised as:

- A single-layer switchable bandpass FSS is presented in this thesis. It has a stable frequency response for oblique TE and TM incidences and can easily be

used to electronically reconfigure the electromagnetic architecture of buildings. The single-layer configuration circumvents the problems of more complicated multi-layer switchable FSS designs presented in the literature.

- The DC biasing in the design of an active FSS is a real challenge. This research has presented two simple and easy to design biasing schemes. Both biasing techniques have been designed to have a minimal effect on the overall electromagnetic behaviour of the active FSS.

- This active FSS, with electronic control, may be used in active radomes, vehicle antennas, active waveguide horns, RCS reduction, reconfigurable reflector systems and WLANs. It may also find use in electronically reconfiguring the electromagnetic architecture of buildings.

7.3 FSS for Energy-Saving Glass

Chapter 5 describes characterisation work that was required as a prerequisite before designing frequency selective surfaces for modern-day energy-saving glass to improve the transmission of wireless/mobile/cellular communication signals through it. The relative permittivity and conductivity of glass has been measured accurately in this work. Chapter 6 presents the practical design of an FSS and its effect on the infrared (heat) and visible (light) properties of the energy-saving glass. These are the contributions arising from these two Chapters.

- Accurate measurements of relative permittivity and conductivity of the glass and the electrical properties of the coating surface were completed for commercial glass samples. These values are essential for a reliable design of band pass

FSS for energy-saving glass. Measurements were completed using a parallel-plate capacitor and waveguide technique.

- The effect of etching an FSS on the transmission of RF/microwave, Infrared (IR) and light (visible) waves for two types of commercial energy-saving glass panels is also analysed. The authors of previous research did not consider this multi-disciplinary aspect of FSS design.

- Practical values of surface resistivity for the glass coating have been used in the simulations. This made it possible to obtain good agreement between the theoretical and measured results. This aspect was not considered in previous research.

- The bandpass FSS can improve the transmission of useful microwave signals (which are normally attenuated) through energy-saving glass while keeping good WLAN security and infrared attenuation.

- One of the publications on this research was awarded best paper prize in a conference (Workshop on Applications of Radio Science (WARS), Gold Coast, Australia, 10th-12th February 2008). Also, a scholarship of worth 12000 Swedish Kronas was awarded to me by Lund University, Sweden, on the successful completion of the glass FSS project.

7.4 Suggestions for Future Research

- The distance between the two layers of absorb/transmit FSS may need to be further reduced to get a more compact design, specially for low-frequency applications.

- In the single-layer active FSS design, the isolation between transmission and reflection states is experimentally about 10 dB. This isolation is not very strong. Research can be carried out to increase the value of the isolation by using better diodes and low-loss substrates. Also, research can be extended by replacing PIN diodes with varactor diodes to achieve a continuous frequency response rather than just two states (as in the case of PIN diodes).

  Despite the advantages of an active FSS with reconfigurable properties, the cost of the product remains a big issue. The cost of active devices such as PIN or varactor diodes in FSS design plays a major role in the final cost. Also, the requirement of a continuous dc supply for diode biasing requires extra investment. Research can be extended to find that how to make a smaller FSS that can serve a larger security area.

- As the wireless technology is changing and new frequency bands are being introduced, the need for a variable FSS filter response will arise with the passage of time. To obtain this variable/switchable frequency response of an FSS, the inclusion of active devices such as PIN or varactor diodes in the energy-saving glass can be investigated.

- For commercial buildings having tubular/curved architecture with energy-saving glass incorporated in the design, the conventional planar FSS designs may not be an applicable filter solution. Therefore, research has to be extended towards the design and development of curved FSSs which is both complex and challenging compared to the design of a planar FSS (as presented in this thesis).

- As the windows of trains and cars are also using energy-saving glass, the FSS filter solution can be extended to this technology as well.

Bibliography

[1] B. A. Munk, *Frequency Selective Surfaces, Theory and Design* (John Wiley & Sons Inc, 2000).

[2] E. A. Parker, S. M. A. Hamdy, and R. J. Langley, "Arrays of concentric rings as a frequency selective surface," Electronics Letters **17,** 880–881 (1981).

[3] G. I. Kiani, A. R. Weily, and K. P. Esselle, "A novel absorb/transmit FSS for secure indoor wireless networks with reduced multipath fading," IEEE Microwave and Wireless Components Letters **16,** 378–380 (2006).

[4] E. A. Parker, S. M. A. Hamdy, and R. J. Langley, "Modes of resonance of the Jerusalem cross in frequency selective surfaces," IEE Proceedings on Microwaves, Antennas and Propagation **130,** 203–208 (1983).

[5] E. A. Parker and B. Savia, "Active frequency selective surfaces with ferroelectric substrates," IEE Proceedings on Microwaves, Antennas and Propagation **148,** 103–108 (2001).

[6] B. Philips, E. A. Parker, and R. J. Langley, "Active FSS in an experimental horn antenna switchable between two beamwidths," Electronics Letters **31,** 1–2 (1995).

[7] B. Chambers and K. L. Ford, "Tunable radar absorbers using frequency selective surfaces," In *Eleventh International Conference on Antennas and Propagation*, pp. 593–597 (2001).

[8] R. L. Fante and M. T. McCormack, "Reflection properties of the Salisbury screen," IEEE Transactions on Antennas and Propagation **36,** 1443–1454 (1988).

[9] F. Smith, "Design principles of broadband adaptive Salisbury screen absorber," Electronics Letters **38,** 1052–1054 (2002).

[10] R. Haupt, "Scattering from small Salisbury screens," IEEE Transactions on Antennas and Propagation **54,** 1807–1810 (2006).

[11] A. Itou, O. Hashimoto, H. Yokokawa, and K. Sumi, "A fundamental study of a thin wave absorber using FSS technology," Electronics and Communications in Japan (Part I: Communications) **87,** 77–86 (2004).

[12] A. Itou, H. Ebara, H. Nakajima, K. Wada, and O. Hashimoto, "An experimental study of a wave absorber using a frequency selective surface," Microwave and Optical Technology Letters **28,** 321–323 (2001).

[13] B. A. Munk, P. Munk, and J. Pryor, "On designing Jaumann and circuit analog absorbers for oblique angle of incidence," IEEE Transactions on Antennas and Propagation **55,** 186–193 (2007).

[14] R. Mittra, C. H. Chan, and T. Cwik, "Techniques for Analyzing Frequency Selective Surfaces - A Review," IEEE Proceedings on Microwaves, Antennas and Propagation **76,** 1593–1615 (1988).

[15] B. Hooberman, "Everything you ever wanted to know about frequency selective surface filters but were afraid to Ask," Technical report (2005) .

[16] C. G. Christodoulou, D. P. Kwan, R. Middleveen, and P. F. Wahid, "Scattering from Stacked Gratings and Dielectrics for Various Angles of Wave Incidence," IEEE Transactions on Antennas and Propagation **36,** 1435–1442 (1988).

[17] R. C. Hall, R. Mittra, and K. M. Mitzner, "Analysis of Multilayered Periodic Structures Using Generalized Scattering Matrix Theory," IEEE Transactions on Antennas and Propagation **36,** 511–517 (1988).

[18] J. D. Vacchione, C. H. Chan, and R. Mittra, "Cascade analysis of power distribution in a multilayered dielectric/Frequency Selective Surface system," In *IEEE AP-S International Symposium Digest*, pp. 1080–1083 (1989).

[19] J. D. Vacchione and R. Mittra, "A generalized scattering matrix analysis for cascading FSS of different periodicities," In *IEEE AP-S International Symposium Digest*, pp. 92–95 (1990).

[20] J. D. Vacchione and T. K. Wu, "Analysis of a dual, non-Similar, screen FSS using simple cascading procedures," In *IEEE AP-S International Symposium Digest*, pp. 1779–1782 (1992).

[21] J. Shaker and L. Shafai, "Analysis of multiresonant Frequency Selective Surfaces," IEEE AP-S International Symposium Digest **3,** 1948–1951 (1993).

[22] J. D. Vacchione, "Techniques for analyzing planar, periodic, frequency selective surface systems," The University of Illinois at Urbana-Champaign, PhD Thesis (1990).

[23] F. S. Johansson, "Analysis and design of double-layered Frequency Selective Surfaces," IEE Proceedings **132,** 319–325 (1985).

[24] B. A. Munk, R. J. Leubers, and R. D. Fulton, "Transmission Through a Two-Layer Array of Loaded Slots," IEEE Transactions on Antennas and Propagation AP-22 (1974).

[25] T. Cwik and R. Mittra, "The Cascade Connection of Planar Periodic Surfaces and Lossy Dielectric Layers to Form an Arbitrary Periodic Screen," IEEE Transactions on Antennas and Propagation **35,** 1397–1405 (1987).

[26] B. A. Munk and R. J. Luebbers, "Reflection Properties of Two-Layered Dipole Arrays," IEEE Transactions on Antennas and Propagation **4,** 766–773 (1974).

[27] P. S. R. Orta and R. Tascone, "A New Class of Frequency Selective Surfaces," In *IEEE AP-S International Symposium Digest*, pp. 1767–1770 (1992).

[28] G. Marconi and C. S. Franklin, "Reflector for use in wireless telegraphy and telephony," US Patent 1,301,473 (1919).

[29] R. Ulrich, "Far-infrared properties of metallic mesh and its complementary structure," Infrared Physics **7,** 37–55 (1967).

[30] V. Galindo and N. Amitay, "The analysis of circular waveguide phased arrays," Bell SystemTech. J 47 (1968).

[31] E. A. Parker, A. D. Chuprin, J. C. Batchelor, and S. B. Savia, "GA optimisation of crossed dipole FSS array geometry," Electronics Letters **37,** 996–997 (2001).

[32] G. I. Kiani, A. R. Weily, and K. P. Esselle, "Frequency selective surface absorber using resistive cross-dipoles," In *IEEE Antenna and Propagation Society International Symposium*, pp. 4199–4202 (2006).

[33] P. W. B. Au, L. S. Musa, E. A. Parker, and R. Langley, "Parametric study of tripole and tripole loop arrays as frequency selective surfaces," IEE Proceedings **137,** 263–268 (1990).

[34] M. M. Mokhtar and E. A. Parker, "Conjugate gradient computation of the current distribution on a tripole FSS array element," Electronics Letters **26,** 227–228 (1990).

[35] J. C. Vardaxoglou and E. A. Parker, "Performance of two tripole arrays as frequency selective surfaces," Electronics Letters **19,** 709–710 (1983).

[36] R. Cahill and E. A. Parker, "Concentric ring and Jerusalem cross arrays as frequency selective surfaces for a 45° incidence diplexer," Electronics Letters **18,** 313–314 (1982).

[37] M. Hosseini, A. Pirhadi, and M. Hakkak, "Design of an AMC with little sensitivity to angle of incidence using an optimized jerusalem cross FSS," IEEE International Workshop on Antenna Technology and Novel Metamaterials pp. 245–248 (2006).

[38] K. Merewether, R. Mittra, T. Cwik, and T. Wu, "Relative convergence of the spectral-Galerkin solution for the frequency response characteristics of the Jerusalem cross FSS," In *IEEE Antenna and Propagation Society International Symposium*, pp. 859–862 (1986).

[39] J. Vardaxoglou, A. Hossainzadeh, and A. Stylianou, "Scattering from two-layer FSS with dissimilar lattice geometries," IEE Proceedings **140,** 59–61 (1993).

[40] C. K. Lee and R. J. Langley, "Compound reflector antennas," IEE Proceedings on Microwaves, Antennas and Propagation **139,** 135–138 (1992).

[41] R. Cahill and E. A.Parker, "Performance of millimetre-wave frequency selective surfaces in large incident angle quasioptical systems," Electronics Letters **28,** 788–789 (1992).

[42] T. K. Wu, "Four-Band frequency selective surface with double-square-loop patch elements," IEEE Transactions on Antennas and Propagation **42,** 1659–1663 (1994).

[43] T. K. Chang, R. J. Langley, and E. Parker, "An active square loop frequency selective surface," IEEE Microwave and Guided Wave Letters **3,** 387–388 (1993).

[44] K. Merewether, R. Mittra, T. Cwik, and T. Wu, "Research on reflection phase characterizations of artificial magnetic conductors," In *Asia-Pacific Microwave Conference*, (2005).

[45] G. I. Kiani, K. L. Ford, K. P. Esselle, and A. R. Weily, "Oblique incidence performance of an active square loop frequency selective surface," In *2nd European Conference on Antennas and Propagation*, (2007).

[46] E. A. Parker and J. C. Vardaxoglou, "Plane wave illumination of concentric ring frequency selective surfaces," IEE Proceedings **132,** 176–180 (1985).

[47] E. A. Parker, C. Antonopoulos, and N. E. Simpson, "Microwave band FSS in optically transparent conducting layers: Performance of ring element arrays.," Microwave and Optical Technology Letters **16,** 61–63 (1997).

[48] T. K. Wu and S. W. Lee, "Multi band frequency selective surface with multi ring elements," IEEE Transactions on Antennas and Propagation **42,** 1484–1490 (1994).

[49] R. Cahill, J. C. Vardaxoglou, and M. Jayawardene, "Two-layer MM-wave FSS of linear slot elements with low insertion loss," IEE Proceedings on Microwaves, Antennas and Propagation **148,** 410–412 (2001).

[50] M. Jayawardene, R. Dickie, J. A. Flint, J. C. Vardaxoglou, R. Cahill, H. S. Gamble, V. F. Fusco, and N. Grant, "Multilayer aperture ring frequency selective surface modelling," In *IEEE Antenna and Propagation Society International Symposium*, pp. 392–395 (2005).

[51] G. I. Kiani, K. L. Ford, K. P. Esselle, A. R. Weily, C. J. Panagamuwa, and J. C. Batchelor, "Single-layer bandpass active frequency selective surface," Microwave and Optical Technology Letters **50,** 2149–2151 (2008).

[52] E. L. Pelton and B. A. Munk, "A streamlined metallic radome," IEEE Transactions on Antennas and Propagation **22,** 799–803 (1974).

[53] C. Winnewisser, F. Lewen, F. Weinzierl, and H. Helm, "Frequency selective surfaces analyzed by THz-time-domain spectroscopy," In *IEEE Sixth International Conference on Terahertz Electronics Proceedings, New York, USA*, pp. 196–198 (1998).

[54] A. Kondo, "Design and characteristics of ring slot type FSS," Electronics Letters **27,** 240–241 (1991).

[55] A. E. Martynyuk and J. I. M. Lopez, "Frequency-selective surfaces based on shorted ring slots," Electronics Letters **37,** 268–269 (2001).

[56] S. Monni, N. L. Juan, A. Neto, and G. Gerini, "A closely spaced waveguide phased array integrated with a frequency selective surface. Modeling and design," In *IEEE Antennas and Propagation Society International Symposium*, pp. 829–832 (2003).

[57] G. Gerini, S. Monni, and L. Zappelli, "Optimal choice of the E.M. expansion for arbitrary shaped aperture/patch FSSs in planar phased arrays," In *IEEE International Symposium on Phased Array Systems and Technology*, pp. 464–469 (2003).

[58] E. Topsakal and J. L. Volakis, "Frequency selective volumes for optical spatial filters," IEEE Antennas and Wireless Propagation Letters **3,** 23–238 (2004).

[59] H. Wakabayashi, M. Kominami, H. Kusaka, and H. Nakashima, "Numerical simulations for frequency selective screen with complementary elements," IEE Proceedings Microwaves, Antennas and Propagation **141,** 477–482 (1994).

[60] J. Shaker and L. Shafai, "Removing the angular sensitivity of FSS structures using novel double layer structures," IEEE Microwave and Guided Wave Letters **5,** 324–325 (1995).

[61] M. Wahid and S. Morris, "Metal radomes reduced RCS performance," GEC Journal of Research **9,** 166–171 (1992).

[62] L. S. Musa, P. W. B. Au, E. A. Parker, and R. Langley, "Sensitivity of tripole and calthrop FSS reflection bands to angle of incidence," Electronics Letters **25,** 284–285 (1989).

[63] G. I. Kiani, K. L. Ford, K. P. Esselle, A. R. Weily, and C. J. Panagamuwa, "Angle and polarization independent bandstop frequency selective surface for indoor wireless systems," Microwave and Optical Technology Letters **50,** 2315–2317 (2008).

[64] N. Amitay, V. Galindo, and C. P. Wu, *Theory and Analysis of Phased Array Antennas* (Wiley-Interscience, New York, 1972).

[65] S. B. Savia and E. A. Parker, "Equivalent circuit model for superdense linear dipole FSS," IEE Proceedings on Microwaves, Antennas and Propagation **150,** 37–42 (2003).

[66] K. Chang, S. il Kwak, and Y. J. Yoon, "Equivalent circuit modeling of active frequency selective surfaces," In *IEEE Radio and Wireless Symposium*, pp. 663–666 (2008).

[67] C. K. Lee and R. J. Langley, "Equivalent-circuit models for frequency selective surfaces at oblique angles of incidence," Proc. Inst. Elect. Eng. **132,** 395–399 (1985).

[68] C. C. Chen, "Transmission of microwave through perforated flat plates of finite thickness," IEEE Transactions on Microwave Theory and Techniques **21,** 1–6 (1973).

[69] J. Blackburn and L. R. Arnaut, "Numerical convergence in periodic method of moments analysis of frequency selective surfaces based on wire elements," IEEE Transactions on Antennas and Propagation **53,** 3308–3315 (2005).

[70] C. C. Chen, "Transmission through a conducting screen perforated periodically with apertures," IEEE Transactions on Microwave Theory and Techniques **18,** 627–632 (1970).

[71] C. C. Chen, "Diffraction of electromagnetic waves by a conducting screen perforated periodically with circular holes," IEEE Transactions on Microwave Theory and Techniques **19,** 475–481 (1971).

[72] C. C. Chen, "Scattering by a two-dimensional periodic array of conducting plates," IEEE Transactions on Antennas and Propagation **18,** 660–665 (1970).

[73] J. P. Montgomery, "Scattering by an infinite periodic array of thin conductors on a dielectric sheet," IEEE Transactions on Antennas and Propagation **23,** 70–75 (1975).

[74] D. H. Dawes, R. C. McPhedran, and L. B. Whitbourn, "Thin capacitive meshes on a dielectric boundary: Theory and experiment," Applied Optics **28,** 3498–3510 (1989).

[75] J. C. Vardaxoglou and A. Stylianou, "Analysis of frequency selective surfaces using a conjugate gradient method," In *7th IEE International Conference on Antennas and Propagation*, pp. 624–627 (1991).

[76] T. K. Wu, *Frequency Selective Surface and Grid Array* (John Wiley & Sons Inc, 1995).

[77] J. P. Montgomery and K. R. Davey, "The solution of planar periodic structures using iterative methods," Electromagnetics **5,** 209–235 (1985).

[78] R. Kastner and R. Mittra, "Iterative analysis of finite-sized planar frequency selective surfaces with rectangular patches or perforations," IEEE Transactions on Antennas and Propagation **35,** 372–377 (1987).

[79] M. N. Vouvakis, K. Zhao, and J. F. Lee, "Finite-element analysis of infinite periodic structures with nonmatching triangulations," IEEE Transactions on Magnetics **42,** 691–694 (2006).

[80] M. N. Vouvakis, K. Zhao, and J. F. Lee, "Finite Element Analysis of Complex Antennas and Arrays," IEEE Transactions on Antennas and Propagation **56,** 2222–2240 (2008).

[81] http://www.ansoft.com/products/hf/hfss (Accessed in March 2009) .

[82] R. Schuhmann and T. Weiland, "The nonorthogonal finite integration technique applied to 2D- and 3D-eigenvalue problems," IEEE Transactions on Magnetics **36,** 897–901 (2000).

[83] S. Yuferev, L. D. Reinzo, and N. Ida, "Surface impedance boundary conditions for the finite integration technique," IEEE Transactions on Magnetics **42,** 823–826 (2006).

[84] http://www.cst.com (Accessed in March 2009) .

[85] http://en.wikipedia.org/wiki/Salisbury_screen (Accessed in March 2009) .

[86] http://en.wikipedia.org/wiki/Jaumann_absorber
(Accessed in March 2009) .

[87] A. Tennant and B. Chambers, "Design of wideband Jaumann radar absorbers with optimum oblique incidence performance," Electronics Letters **30,** 1530–1532 (1994).

[88] A. McCowen, A. Charles, and M.S.Towers, "Sensitivity analysis of Jaumann absorbers," IEE Proceedings on Microwaves, Antennas and Propagation **146,** 258–262 (1999).

[89] M. Gustafsson, A. Karlsson, A. P. P. Rebelo, and B. Widenberg, "Design of frequency selective windows for improved indoor outdoor communication," IEEE Transactions on Antennas and Propagation **54,** 1897–1900 (2006).

[90] B. Widenberg and J. V. Rodriguez, "Design of energy saving windows with high transmission at 900 MHz and 1800 MHz," Technical Report No. LUTEDX/(TEAT-7110), Lund Institute of Technology (2002) .

[91] D. K. Cheng, *Field and Wave Electromagnetics*, 2nd ed. (Addison-Wesly, 1989).

[92] C. Mias, C. Tsakonas, and C. Oswald, "An investigation into the feasibility of designing frequency selective windows employing periodic structures," Technical Report No. AY3922, The Nottingham Trent University, UK (2001) .

[93] E. A. Parker and S. Massey, "Application of FSS structures to selectively control the propagation of signals into and out of buildings," Technical Report No. Annex 3 (2004) .

[94] F. Terracher and G. Berginc, "Thin electromagnetic absorber using frequency selective surfaces," In *IEEE Antenna and Propagation Society International Symposium*, pp. 846–849 (2000).

[95] A. Tennant and B. Chambers, "A single-layer tuneable microwave absorber using an active FSS," IEEE Microwave and Guided Wave Letters **14,** 46–47 (2004).

[96] B. M. Cahill and E. A. Parker, "Field switching in an enclosure with active FSS screen," Electronics Letters **37,** 244–245 (2001).

[97] C. Mias, "Frequency selective surfaces loaded with surface-mount reactive components," Electronics Letters **39,** 724–726 (2003).

[98] A. C. Lima, E. A. Parker, and R. J. Langley, "Tunable frequency selective surface using liquid substrates," Electronics Letters **20,** 281–282 (1994).

[99] A. E. Martynyuk, J. I. M. Lopez, and N. A. Martynyuk, "Active frequency-selective surfaces based on loaded ring slot resonators," Electronics Letters **41,** 2–4 (2005).

[100] K. Mitchell, A. Keen, L. Davenport, C. Smartt, P. Leask, R. Larson, and J. Davies, "Research to demonstrate the ability of close-coupled frequency selec-

tive structures to enhance the spectral efficiency of radio systems in buildings," Technical Report No. AY4462B (2004) .

[101] M. Philippakis, "Application of FSS structures to selectively control the propagation of signals into and out of buildings," Technical report, ERA Technology, Cleeve road, Leatherhead, Surrey, KT22 7SA, U.K (2004) .

[102] http://www.wi-fiplanet.com/tutorials/article.php/1569271 (Accessed in March 2009) .

[103] A. P. Raiva, F. J. Harackiewicz, and J. Lindsey, "Frequency Selective Surfaces: Design of broadband elements and new frequency stabilization techniques," In *Antenna application symposium, Monticello, Illinois*, (2003).

[104] http://www.ohmega.com/OhmPly.html (Accessed in March 2009) .

[105] G. F. Engen and C. A. Hoer, "Thru-reflect-line: An improved technique for calibrating thc dual six-port automatic network analyser," IEEE Transactions on Microwave Theory and Techniques **27,** 987–993 (1971).

[106] P. Hannan and M. Balfour, "Simulation of a phased-array antenna in Waveguide," IEEE Transactions on Antennas and Propagation **13,** 342–353 (1965).

[107] D. M. Pozar, *Microwave Engineering* (John Wiley & Sons Inc, 2004).

[108] S. J. Orfanidis, *Electromagnetic Waves and Antennas* (ECE Department, Rutgers University, NJ, USA, 2008).

[109] http://www.ee.kent.ac.uk/research/theme_project.aspx?pid=84 (Accessed in March 2009) .

[110] E. Parker, J. B. Robertson, S. Lzquierdo, and J. Batchelor, "Minimal size FSS for long wavelength operation," Electronics Letters **44,** 394–395 (2008).

[111] http://www.nxp.com/acrobat_download/datasheets/BAP51-03_4.pdf (Accessed in March 2009) .

[112] http://www.elektrosmog.de/Gutachten/HyperLOG7000-E.pdf (Accessed in March 2009) .

[113] http://www.pilkington.com (Accessed in March 2009) .

[114] A. V. Hippel, *Dielectric Materials and Applications* (Artech House, Boston, London, 1995).

[115] http://www.pilkington.com/applications/products2006/english/bybenefit/thermalinsulation/optitherm/default.htm (Accessed in March 2009) .

[116] www.pilkington.com/applications/products2006/english/bybenefit/solarcontrol/suncool/default.htm (Accessed in March 2009) .

[117] http://www.lpkfusa.com/RapidPCB/CircuitboardPlotters/95sii.htm (Accessed in March 2009) .

[118] http://www.surplusserver.com/PDF/Lambda800_900_Brochure.pdf (Accessed in March 2009) .

Appendix: Waveguide Measurement Technique

The block diagram and the setup are depicted in Figs 1 and 2. An X-band waveguide (WR-90) with cross-section $a \times b = 22.86$ mm $\times$ 10.16 mm was used, with TE_{10} as the fundamental propagating mode. The frequency range of such a system is 6.6 to 13.1 GHz, corresponding to the frequency band where only the fundamental mode is propagating. The accuracy of the measurements is important, and for this reason measurements were only done in the frequency band of 9 to 10 GHz. It is difficult to obtain good accuracy outside this band [114].

In the waveguide measurements it is crucial that the device under test is shaped such that it fits exactly into the waveguide. A small air gap between the glass and the waveguide invalidates the results. The glass sample is placed in the waveguide, well pressed against the shortening plate. A standing-wave meter is used for measuring the location of the voltage minima with and without a glass sample. It is also used for measuring the corresponding 3 dB widths of the voltage minima. Here a method was used, to measure high values of VSWR (>10), that circumvents the problem of determining the precise value of a deep minimum. The VSWR is defined as:

$$S = \frac{V_{max}}{V_{min}} = \sqrt{\frac{P_{max}}{P_{min}}} = \sqrt{\frac{I_{Dmax}}{I_{Dmin}}}$$

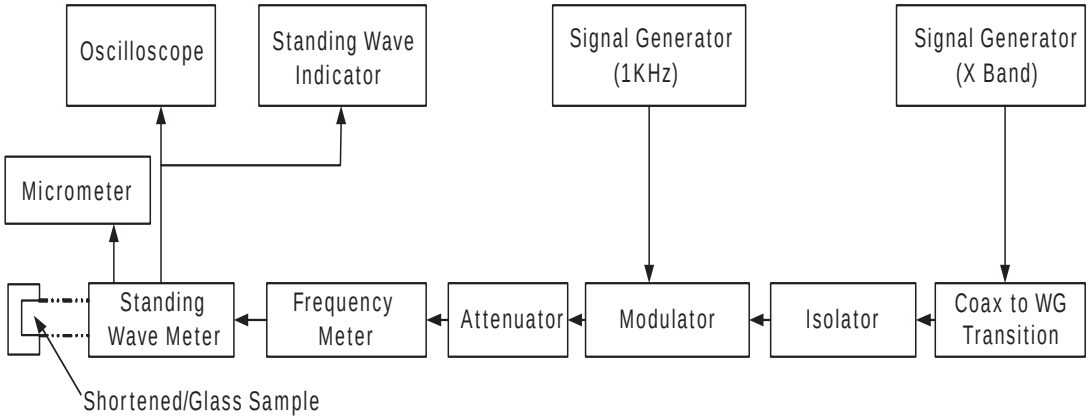

Figure 1 Block diagram showing the waveguide measurement method.

when measured with an ordinary quadratic detector diode (where I_{Dmax} and I_{Dmin} are maximum and minimum diode currents, V_{max} and V_{min} are maximum and minimum diode voltages and P_{max} and P_{min} are maximum and minimum diode powers). If studied on a linear scale, the SWR pattern is described by $\cos 2\beta z$. This pattern, thus, is sinusoidal and can be represented on a circle with circumference $\lambda_g/2$ where λ_g is the guided wavelength. Utilising the theorem of intersecting chords and some other geometric theorems, the VSWR can be calculated as $\lambda_g/\pi d$, d being the distance around the circle between the two points where the diode current is twice its minimum. This is equivalent to finding the distance between the points where the power is $2P_{min}$ or 3 dB above the minimum. These points are easily found with a common slotted line, rather than the deep minimum itself [114]. From these measured values the permittivity and conductivity of the glass can be calculated as follows.

Measurement of Permittivity

Referring to Fig. 3, a coordinate system x, y, z is considered such that the waveguide occupies $0 < x < a$, $0 < y < b$, $z \geq 0$. The shorted plane is at $z = 0$ such that the glass sample occupies $0 < z < z_0$. The incident waveguide mode is the fundamental

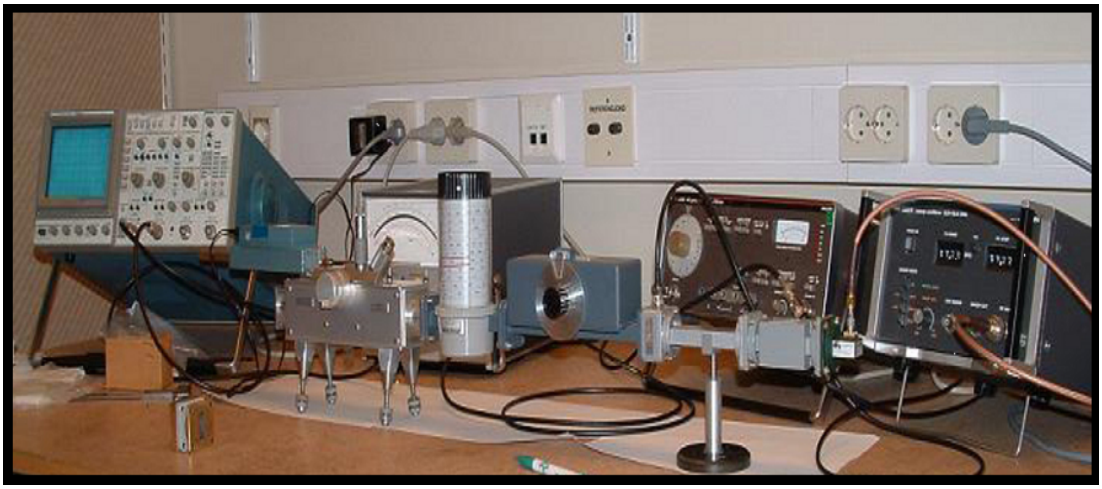

Figure 2 Waveguide measurement setup.

mode with electric and magnetic field components:

$$\begin{aligned}\vec{E}(x,z) &= E_0 \sin(\pi x/a) e^{-ik_z z}\hat{y} \\ \vec{H}(x,z) &= E_0 \frac{k_z}{\omega\mu_0} \sin(\pi x/a) e^{-ik_z z}\hat{x} - i\frac{\pi}{\omega\mu_0 a} E_0 \cos(\pi x/a) e^{-ik_z z}\hat{z}\end{aligned} \tag{1}$$

Here $k_z = \sqrt{k^2 - (\pi/a)^2} = \sqrt{(\omega/c_0)^2 - (\pi/a)^2}$, is the z-component of the wave vector and $c_0 = 1/\sqrt{\mu_0 \varepsilon_0}$ is the speed of light in vacuum. The cut-off frequency is $f_c = c/2a$.

The total electric and magnetic fields are decomposed in their longitudinal component ((E_z, H_z) and transverse component ($\vec{E}_T$, $\vec{H}_T$). In the area $z > z_0$ the fields are

$$\vec{E}(x,z) = E_0 \sin(\pi x/a)(e^{-ik_z z} + Re^{ik_z z})\hat{y}$$

$$\vec{H}(x,z) = \vec{H}_T(x,z) + H_z(x,z)\hat{z}$$

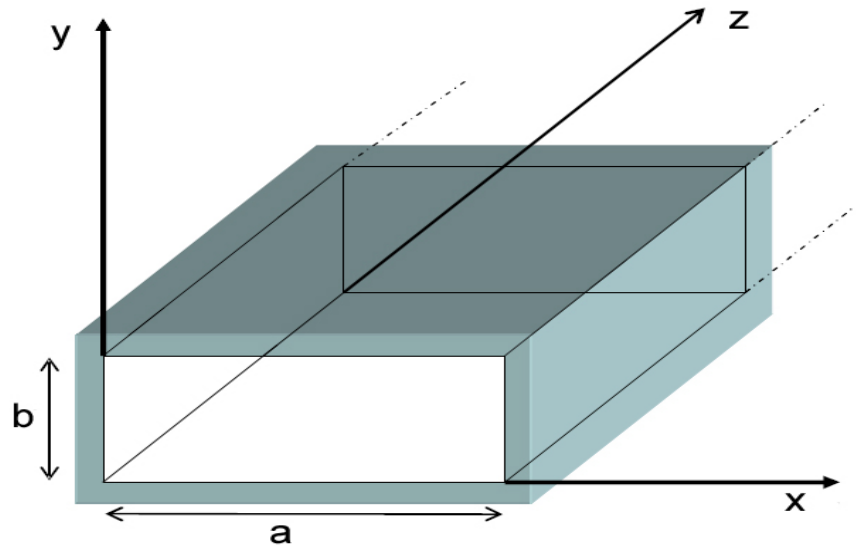

Figure 3 X-band waveguide illustration.

where R is the reflection coefficient and

$$\vec{H}_T(x,z) = E_0 \frac{k_z}{\omega\mu_0} \sin(\pi x/a)(e^{-ik_z z} - Re^{ik_z z})\hat{x}$$
$$H_z(x,z) = -\frac{i\pi}{\omega\mu_0 a} E_0 \cos(\pi x/a)(e^{-ik_z z} + Re^{ik_z z})$$

In the region $0 < z < z_0$ the corresponding fields are

$$\vec{E}(x,z) = \kappa \sin(\pi x/a)\sin(k'_z z)\hat{y}$$
$$\vec{H}(x,z) = \vec{H}_T(x,z) + H_z(x,z)\hat{z}$$
$$= i\frac{\kappa k'_z}{\omega\mu_0}\sin(\pi x/a)\cos(k'_z z)\hat{x} - i\frac{\kappa\pi}{a\omega\mu_0}\cos(\pi x/a)\sin(k'_z z)\hat{z}$$

where $k'_z = \sqrt{(k')^2 - (\pi/a)^2}$ and κ is an unknown coefficient. Notice that the boundary condition $E_z = 0$ at $z = 0$ is satisfied by this field. The wave number k' is given by

$$k' = \omega\sqrt{\mu_0\varepsilon_c}$$

where the complex permittivity of the sample is given by

$$\varepsilon_c = \varepsilon_0 \varepsilon_r - i\sigma/\omega$$

If the glass sample has non-zero conductivity, then k_z' is a complex number even above the cut-off frequency. Therefore k_z' can be decomposed in to its real and imaginary parts

$$k_z' = \beta - i\alpha$$

The unknown coefficients κ and R are determined from the boundary conditions at $z = z_0$, i.e.

$$\vec{E}(x, z_0^-) = \vec{E}(x, z_0^+)$$

$$\vec{H}_T(x, z_0^-) = \vec{H}_T(x, z_0^+)$$

This gives a system

$$\kappa \sin(k_z' z_0) = E_0(e^{-ik_z z_0} + Re^{ik_z z_0})$$

$$\kappa i k_z' \cos(k_z' z_0) = E_0 k_z (e^{-ik_z z_0} - Re^{ik_z z_0})$$

From this system it follows that

$$\begin{aligned} R &= \frac{k_z \sin(k_z' z_0) - ik_z' \cos(k_z' z_0)}{k_z \sin(k_z' z_0) + ik_z' \cos(k_z' z_0)} e^{-2ik_z z_0} \\ &= \frac{k_z k_z'^{-1} \tan(k_z' z_0) - i}{k_z k_z'^{-1} \tan(k_z' z_0) + i} e^{-2ik_z z_0} \end{aligned} \tag{2}$$

The standing-wave ratio (SWR) is given by

$$SWR = \frac{1 + |R|}{1 - |R|}$$

i.e.

$$|R| = \frac{SWR - 1}{SWR + 1}$$

The first maximum of the pattern occurs at z_b, which is given by

$$Re^{2ik_z z_b} = |R| \tag{3}$$

This means that the complex permittivity can be deduced from the equation

$$R = \frac{SWR - 1}{SWR + 1} e^{-2ik_z z_b} \tag{4}$$

This is done utilizing a numerical method that can find complex roots to equations.

Determination of SWR

Measuring the position for the node (minimum) in the standing wave pattern (please see Fig 4) we get

$$E_{min} = E_0(1 - |R|)$$

Now measure the positions for the two 3 dB levels on both sides of the node, i.e. where $|E| = 2E_{min}$, and let Δ be the distance between these two positions, as in Fig. 4. Then

$$\begin{aligned} |E_{3dB}|^2 &= E_0^2|(1 - |R|e^{ik_z\Delta})|^2 = E_0^2|((1 - |R|\cos(k_z\Delta)) - i|R|\sin(k_z\Delta))|^2 \\ &= E_0^2(1 + |R|^2 - 2|R|\cos(k_z\Delta)) \end{aligned}$$

Since $|E_{3dB}|^2 = 2E_{min}^2$ we get

$$1 + |R|^2 - 2|R|\cos(k_z\Delta) = 2(1 - |R|)^2$$

and then R is given by

$$|R| = 2 - \cos(k_z\Delta) - \sqrt{(\cos(k_z\Delta) - 2)^2 - 1}$$

Now suppose that the losses in the waveguide are considered (due to ohmic losses in the walls). Therefore, the wave is also attenuated in a waveguide filled with air, although the attenuation is very small. In a waveguide without glass sample we have $R = -1$ and the electric field is given by ($x = a/2$)

$$E(z) = E_0(e^{\alpha z}e^{-ik_z z} - e^{-\alpha z}e^{ik_z z}) = E_0 e^{\alpha z}e^{-ik_z z}(1 - e^{-2\alpha z}e^{2ik_z z})$$

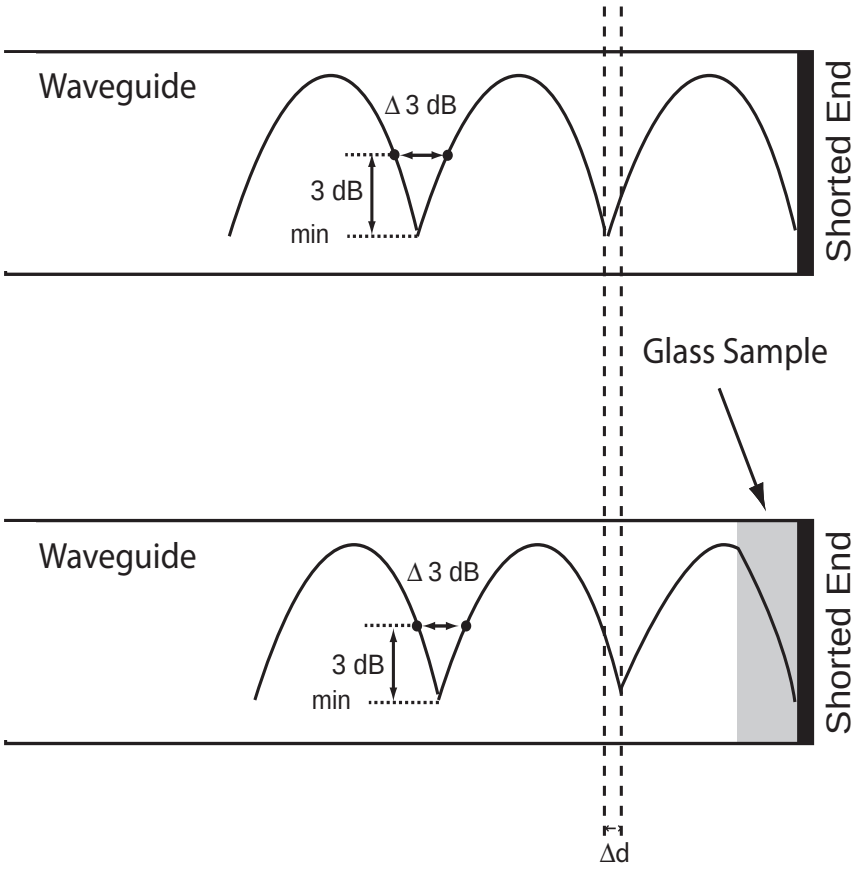

Figure 4 Standing-wave patterns with and without glass sample. The distance Δ d and the difference in distance between two corresponding Δ 3 dB values give the conductivity and permittivity of the glass sample.

Hence the same measurement of SWR can be done as above, which gives

$$e^{-2\alpha z_n} = 2 - \cos(k_z\Delta) - \sqrt{(\cos(k_z\Delta) - 2)^2 - 1}$$

where it is assumed that $e^{-2\alpha\Delta} \approx 1$.

For the waveguide with glass sample

$$E(z) = E_0(e^{\alpha z}e^{-ik_z z} + Re^{-\alpha z}e^{ik_z z}) = E_0 e^{\alpha z}e^{-ik_z z}(1 + Re^{-2\alpha z}e^{2ik_z z})$$

Following the same method as above we get

$$|R|e^{-2\alpha z'_n} = 2 - \cos(k_z\Delta') - \sqrt{(\cos(k_z\Delta') - 2)^2 - 1}$$

where z'_n is the position of the node in the waveguide with the sample and Δ' is the distance between the 3 dB positions. Assuming that the positions of the nodes with and without the sample are close enough to each other that $e^{-2\alpha(z_n - z'_n)} \approx 1$ (the sample needs to be thin), then

$$|R| = \frac{(2 - \cos(k_z\Delta') - \sqrt{(\cos(k_z\Delta') - 2)^2 - 1})}{2 - \cos(k_z\Delta) - \sqrt{(\cos(k_z\Delta) - 2)^2 - 1}}$$